RESEARCH ARTICLE

Dyke to sill deflection in the shallow heterogeneous crust during glacier retreat: part I

Kyriaki Drymoni[1,2] · Alessandro Tibaldi[1,3] · Fabio Luca Bonali[1,3] · Federico Aligi Pasquarè Mariotto[4]

Abstract

Dykes and sills occupy Mode I (extension), Mode II (shear), or hybrid mode fractures and most of the time transport and store magma from deep reservoirs to the surface. Subject to their successful propagation, they feed volcanic eruptions. Yet, dykes and sills can also stall and become arrested as a result of the crust's heterogeneous and anisotropic characteristics. Dykes can become deflected at mechanical discontinuities to form sills, and vice versa. Although several studies have examined dyke propagation in heterogeneous and anisotropic crustal segments before, the conditions under which dykes propagate in glacial-volcanotectonic regimes remain unclear. Here, we coupled field observations with 2D FEM numerical modelling to explore the mechanical conditions that encourage (or not) dyke-sill transitions in volcanotectonic or glacial settings. We used as a field example the Stardalur cone sheet-laccolith system, which lies on the Esja peninsula, close to the western rift zone, NW of the southern part of the Icelandic rift. The laccolith is composed of several vertical dykes that transition into sills and form a unique stacked sill 'flower' structure. Here, we investigate whether the Stardalur laccolith was formed under the influence of stresses caused by glacial retreat due to thickness variations (0–1 km) in addition to regional and local tectonic stresses (1–3 MPa extension or compression) and varied magma overpressure (1–30 MPa), as well as the influence of the mechanical properties of the lava/hyaloclastite contact. Our results show that the observed field structure in non-glacial regimes was formed as a result of either the mechanical (Young's modulus) contrast of the lava/hyaloclastite contact or a compressional regime due to pre-existing dykes or faulting. In the glacial domain, the extensional stress field below the ice cap encouraged the formation of the laccolith as the glacier became thinner (subject to a lower vertical load). In all cases, the local stress field influenced dyke to sill deflection in both volcanotectonic regimes.

Keywords Dyke-sill deflection · Stardalur laccolith · Iceland · FEM numerical modelling · Glacier retreat

✉ Kyriaki Drymoni
kyriaki.drymoni@min.uni-muenchen.de

1 Department of Earth and Environmental Sciences, University of Milan-Bicocca, 20126 Milan, Italy

2 Earth and Environmental Sciences, Ludwig-Maximilians-Universität in Munich, Theresienstr.41, 80333 Munich, Germany

3 CRUST-Interuniversity Center for 3D Seismotectonics With Territorial Applications, 66100 Chieti Scalo, Italy

4 Department of Human and Innovation Sciences, Insubria University, Como, Italy

Introduction

Dyking is the prime mechanism by which magma is transferred from its source to the surface and represents a key component of the magmatic plumbing system of a volcano (Pollard and Johnson 1973; Gudmundsson 2011, 2020; Tibaldi 2015; Cashman et al. 2017; Acocella 2021; Gudmundsson et al. 2022). Dyke-fed eruptions pose a great threat to settlements near a volcano (Guest and Murray 1979; Walker 1982; Gurioli et al. 2010), and therefore, it is necessary to understand the physics that controls magma propagation in the shallow crust. Most of our understanding of dyke injection and the volcano's plumbing system comes from monitoring volcano deformation (Fedotov 1981; Plateaux et al. 2014; Ágústsdóttir et al. 2016; Ebmeier et al. 2018; White et al. 2019; Lundgren et al. 2020; Mullet and Segall 2022), but further valuable insights can be gained

by studying the fossilized remnants of magmatic plumbing systems (Gudmundsson 2011; Tibaldi et al. 2013; Burchardt 2008, 2018; Drymoni 2020; Acocella 2021; Clunes et al. 2023). It is known that the properties of crustal rocks influence the pathways that magmatic fractures take when propagating to the surface (Gudmundsson 2006, 2020; Letourneur et al. 2008; Kavanagh et al. 2017; Browning et al. 2021; Drymoni et al. 2023). Volcanoes made of different rock types and properties can possess highly anisotropic stress fields (Koulakov et al. 2009). The consequence of a highly varied stress field is that dykes can stall at depth (Pinel and Jaupart 2004; Menand 2011; Sulpizio and Massaro 2017; Kavanagh 2018; Kavanagh et al. 2018; Drymoni et al. 2020; Tibaldi et al. 2022). Dykes may also change their pathways dramatically when they encounter unfavourable stresses or intersect pre-existing fractures or faults (Gudmundsson 1984; Jolly and Sanderson 1997; Valentine and Krogh 2006; Gaffney et al. 2007; Browning and Gudmundsson 2015a, b; Spacapan et al. 2016; Healy et al. 2018; Dering et al. 2019; Drymoni et al. 2021, 2022). This behaviour makes it extremely difficult to predict if an injected dyke will reach the surface to feed an eruption or not (Gudmundsson and Brenner 2005; Caricchi et al. 2021). This problem is aggravated in glacial-volcanotectonic regions and in subglacial volcanoes. Long-term climatic effects (Shackleton 1987), such as sea-level changes (McGuire et al. 1997) and ice loading (Glazner et al. 1999), have been shown to influence volcanic activity (Jellinek et al. 2004; Sinton et al. 2005). Loading of the crust by ice sheets contributes to the dynamic, and commonly complex, crustal stresses within subglacial volcanoes (Morner 1978; Hall 1982; Gudmundsson 1986; Stewart et al. 2000; Sigmundsson et al. 2010; Bakker et al. 2016; Wilson and Russell 2020).

Magma propagation in subglacial volcanotectonic environments, as opposed to in subaerial settings, is relatively poorly studied and therefore challenging to elucidate. Subglacial volcanism involves magma vesiculation combined with fast cooling from the magma and ice interaction, producing both effusive and explosive products (Allen 1980). Sequences of glacial and interglacial periods on Earth, mainly affected by orbital variations (Milankovitch 1930; Hays et al. 1976; Huybers and Wunch 2005; Lee et al. 2017), have produced glacial loading and unloading (glacial rebound) conditions, which influence the production of magma (Jull and McKenzie 1996; Maclennan et al. 2002) and its trajectory in the crust (Gudmundsson 1986). These factors also influence the shallow plumbing system (Albino et al. 2010) and produce land elevation (Grapenthin et al. 2006), new fractures (Bovis 1990), or slope instabilities (Eberhardt et al. 2004; Cossart et al. 2008).

In this numerical study, we explore fossilised dyke propagation pathways in glacial-volcanotectonic regimes in the vicinity of the Langjökull glacier (SW Iceland). We studied

the Stardalur laccolith, a stacked sill structure that formed by a series of vertical dykes that transformed into sills (Tibaldi and Pasquaré 2008). A similar nested 'flower structure' has been found at the nearby Thverfell magmatic system (Tibaldi et al. 2008). Unravelling the mechanism responsible for the formation of these nested structures will provide key insights into dyke deflection. Moreover, in Iceland, several major glacial phases occurred so far (Geirsdottir and Eiríksson 1994; Eiríksson 2008); thus, it is worth investigating the possible relationships between sill emplacement and glacier unloading.

In this part (part I), we model dyke-sill transition scenarios that relate to our field-based example, the Stardalur laccolith, and investigate the processes that formed its geometry while a follow-up article (Drymoni et al., in review) expands on the host rock mechanical and geometrical conditions that encourage similar pathways. Here, we design a series of models to understand how the magma overpressure, the local stress field (extension or compression), and the presence of a very weak contact affect dyke to sill deflection. We finally model unloading concepts subject to glacier thickness variations. Our study attempts to answer the following research questions: (1) What mechanical processes formed the Stardalur laccolith: local stresses or glacio-isostatic deformation? (2) How does the magma overpressure, local extension or compression, and the presence of a mechanically weak contact influence the dyke to sill transition in the shallow crust? and (3) How does unloading due to glacier thinning influence the dyke pathways below an ice cap? Our models may be applied universally to volcanoes that experience changes in glacier thickness variations and sill emplacement.

Mechanics of glacier retreat and its effect on volcanism

Fissure eruptions occur in response to crustal bending and uplift above a reservoir that experiences magmatic pressure increase, a condition that can occur during glacial rebound (Gudmundsson 1986; Jellinek et al. 2004). Many areas experience repeated cycles of glaciation such that glaciers grow and shrink with time. Prime examples are the subglacial volcanoes beneath the Eyjafjallajökull, Mýrdalsjökull, and Vatnajökull glaciers in Iceland (Magnússon et al. 2005) and the Pichillancahue-Turbio or Michinmahuida glaciers that overlie sections of volcanic complexes in Chile (Rivera et al. 2012). Mechanically, glaciers advance, erode, and retreat periodically (Sigvaldason and Steinthórsson 1974; Grämiger et al. 2017). This cyclic loading can generate crustal fractures or reactivate pre-existing ones (Gudmundsson 1999), but also increases the degree of mantle melting, hence the volume of the produced magma (Hardarson and Fitton

1991) and the likelihood of the eruptive activity (Huybers and Langmuir 2009; Pagli and Sigmundsson 2008) (Fig. 1a).

Two models describe the relationship between glacier retreat and volcanism. The first one offers a mechanical interpretation using analytical models where the compressive bending stress at the bottom of the crust and atop the magma chamber when ice retreat occurs is high enough to overcome the tensile strength of the host rock. As such, the temporary excess pressure rises, and dyke initiation is favoured (Gudmundsson 1986). This model has subsequently been expanded and refined using numerical methods (Andrew and Gudmundsson 2007). The second model relies on a combined axisymmetric solution and a thermodynamic model, showing that decompression during deglaciation increases the average melting rate and eruption rates in some parts of a rift system (Jull and McKenzie 1996). Both analytical solutions provided crucial insights into the mechanical

aspects of glacier retreat and relate to the formation of shield volcanoes. Specifically, they improved our knowledge of the mechanical formation of the volcanotectonic systems and the formation of the fissures under decompression by identifying the volume of melt (or magma) (Vm), the volume of the magma reservoir (Vb), the tensile bending stress (σb) of the glacier cap, and the excess magmatic pressure (Pe) needed for a maximum crustal uplift atop a shallow magma chamber (Fig. 1b).

However, the stress fields and mechanical properties of those systems are significantly more complex. Glacial unloading is not a simple bending/unbending process, but it can instead alter the stress field in all of the different units below it (Stewart et al. 2000). Therefore, the effects on the shallow plumbing system have not been adequately investigated and remain extremely interesting, timely, and important.
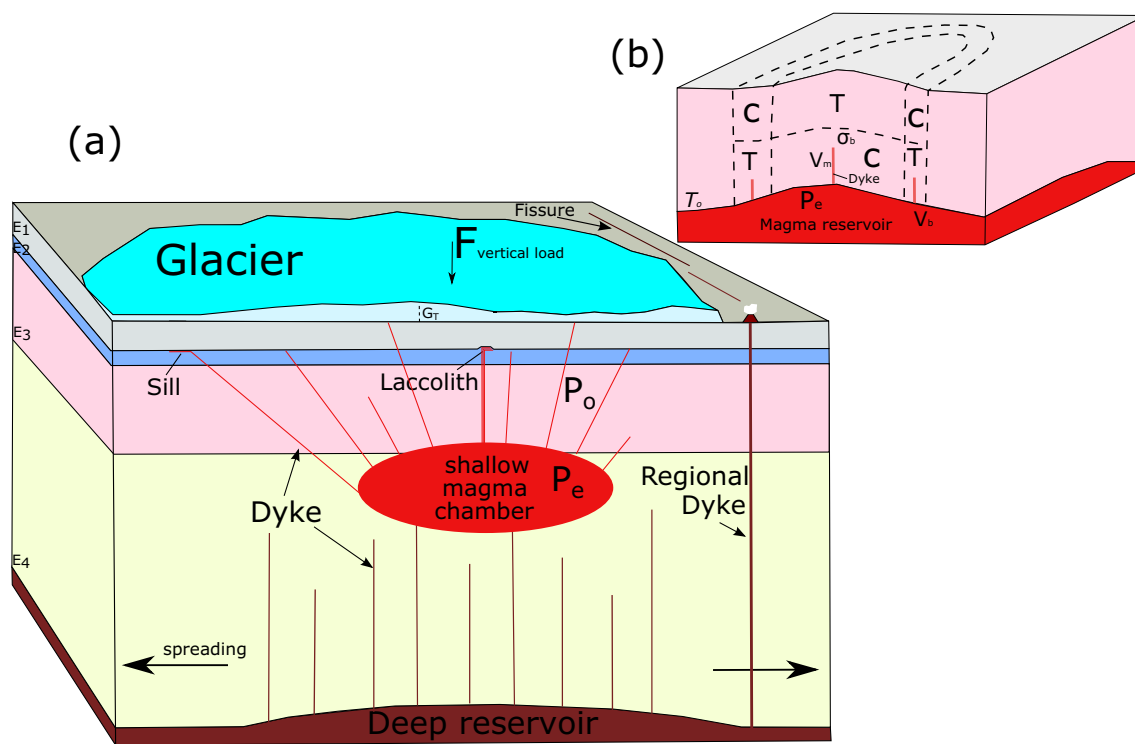

Fig. 1 a A sub-glacial volcanic plumbing system, modified from Browning and Gudmundsson (2015a, b). The deep-seated reservoir feeds a shallow magma chamber. The shallow magma chamber injects dykes and inclined sheets, which follow different pathways subject to their location and the local stress field. F is the vertical load of the glacier associated with the glacier's thickness (G_T), P_o is the overpressure of the dyke, P_e is the excess magma chamber pressure, and E is the Young's modulus of the layer(s). **b** The general stress field above a magma reservoir, modified from Gudmundsson (1986), where uplift and bending of the crust exists when glacier

retreat occurs. C is the compressive stress, T is the tensile stress, T_o is the tensile strength of the host rock, P_e is the excess pressure of the magma reservoir/chamber, Vm is the volume of the melted magma, V_b is the volume of the magma reservoir, and σ_b is the tensile bending stress of the crust. The dashed lines denote the edge of the region subject to bending; the part in the middle shows where tensile stresses are induced during uplift. In the system, three dykes initiate from the magma reservoir at three different locations where different stress fields exist

Regional geology

Geotectonic setting

Iceland was built from the interaction of a mantle plume with a divergent plate boundary (Schilling 1973; Björnsson 1985; Gudmundsson 2000; Schilling et al. 2006; Jacoby and Gudmundsson 2007). In these tectonic settings, where regional stress (σ_{max}) is vertical, dyke propagation is encouraged, though sills have also been emplaced since Miocene times (Burchardt et al. 2022). Iceland's geology is marked by successions of Tertiary basalts that border the active rift system crossing the island from SW to NNE. The Tertiary basaltic lava pile gently dips toward the rift due to the progressive subsidence caused by the loading of the rift zone crust (Pálmason 1980). Petrogenetic studies in the region have revealed that rhyolitic magmas are produced by assimilation of crust-derived partial melts in conjunction with crustal recycling of altered (water-rich) basalts (Jakobsson 1972; Óskarsson et al. 1982, 1985; Thordarson and Larsen 2007).

Our work focuses on the Esja peninsula, located between the western rift zone and the Tertiary basalts that occur NW of the rift. This zone features a succession of 3.3–0.8 Ma basaltic lavas and hyaloclastites known as the Plio-Pleistocene Formation in the geological map of Iceland by Johannesson and Saemundsson (1998). All the lava units, with a total thickness of 1300 m and representing the core of the Esja peninsula, were erupted 2.8, 2.0, and 1.7 Ma ago (Thordarsson and Hoskuldsson 2002). During hiatuses in volcanic activity, the peninsula was affected by glacial erosion, exposing the internal structure of two main shallow magmatic complexes, Stardalur and Thverfell (Tibaldi and Pasquaré 2008; Tibaldi et al. 2008). From about 0.8 Ma ago, volcanic activity resumed on the Esja plateau, leading to the buildup of the Mossfelssheidi basaltic shield volcano, which outpoured lava flows that reached the coastline.

Focusing particularly on the Stardalur complex, detailed lithostratigraphic and structural mapping (at the 1:10,000 scale, Fig. 2a) revealed a succession of basaltic lavas, hyaloclastites, volcano/sedimentary breccias, and fluvial deposits belonging to the older units of the Plio-Pleistocene Formation (Pasquarè and Tibaldi 2007). The succession was cut by several intrusions and covered by lavas < 0.8 Ma old. The intrusions include dykes, inclined sheets, and a major intrusive body, considered a laccolith by Fridleifsson (1977). In the Esja area, at the Stardalur volcanic complex in particular, lies an association of a multiple-sill laccolith nested within a swarm of centrally dipping sheets (Fig. 2a–c) (Pasquarè and Tibaldi 2007; Tibaldi et al. 2008; Tibaldi and Pasquaré 2008). Dykes and inclined sheets are composed of grey-brown dolerite. Dykes and faults mainly trend E–W and NNE–SSW. The NNE–SSW structures are primary dykes and normal faults associated with the main Icelandic rift and are commonly found across most of Iceland.

Glacier retreat and erosional processes in the Esja peninsula

Glaciers are the fingerprints of an area's local climate and landscape evolution as they record its spatial and dynamic development over time (Roe et al. 2017). Climate change, and especially the increasing warming since the twentieth century (Haeberli and Beniston 1998), produces glacier retreat, which subsequently induces glacio-isostatic changes (Jamieson 1865) and crustal deformation due to load adjustments (Harris et al. 1997; Stewart et al. 2000; Larsen et al. 2005; Pagli et al. 2007; Pagli and Sigmundsson 2008; Heimdal et al. 2018; Gaynor et al. 2022). As such, glacial rebound can cause sea level changes (Douglas 1997), increment erosion (Hallet et al. 1996), magma upwelling due to decompression (Jull and McKenzie 1996), and fault instability (Arvidsson 1996; Stewart et al. 2000) that can subsequently increase the local seismicity (Hunt and Malin 1998; Lund Snee and Zoback 2020). In particular, the crustal flexure during glacier retreat can affect volcanism by changing the stress field around magma chambers (Gudmundsson 1986), altering the crustal strain (James and Bent 1994) and the vertical load by encouraging dyke propagation towards the surface (Andrew and Gudmundsson 2007).

Iceland is geographically one of the areas where subglacial eruptive activity plays an essential role in the evolution of volcanism but also controls the movement of magma from the source to the surface. In the rift zones of Iceland, average eruption rates after the end of the last glacial period (12 kyr BP) were up to 100 times higher than those from the glacial period (Maclennan et al. 2002). Volcanological studies on Icelandic volcanoes related to subglacial eruptions to date have mainly focused on the western Vatnajokull ice cap and the Myrdalsjokull glacier nearby. Historical eruptions that occurred in the area are the short-lived 1983 Grimsvotn eruption (Grönvold and Jóhannesson 1984), the 1996 Gjalp eruption, which occurred under the Vatnajokull ice sheet due to a feeder dyke (Gudmundsson et al. 2004), and the Bardarbunga-Holuhraun 2014 eruption (Browning and Gudmundsson 2015a, b; Sigmundsson et al. 2015; Li et al. 2022), which was fed by a more than 45-km lateral dyke and was associated with caldera collapse (Gudmundsson et al. 2016). Data collection from their eruptive products provided invaluable insights into the eruption dynamics, timescales of eruptions, and eruption magnitudes. At the same time,
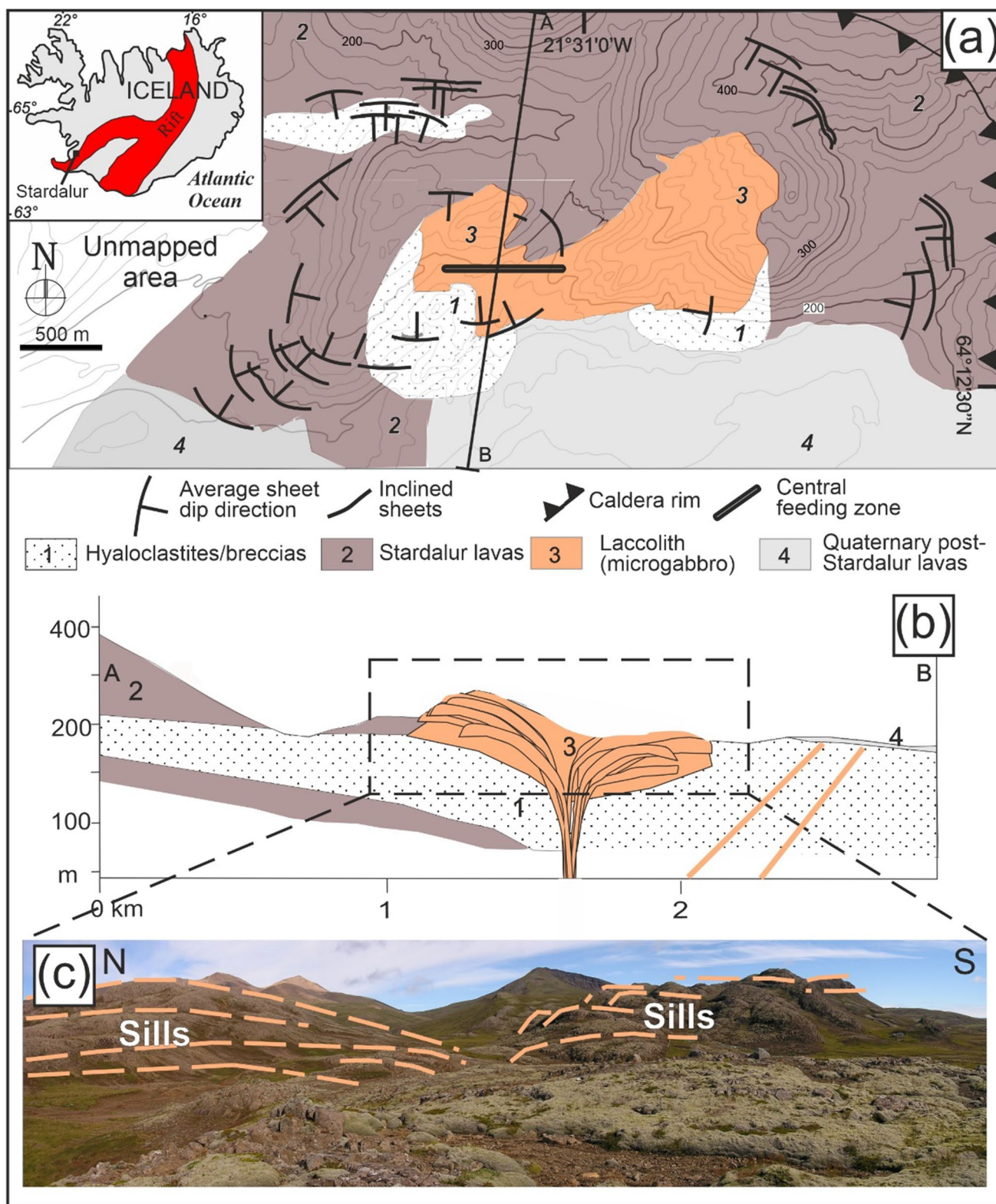
Fig. 2 **a** Simplified sketch of the original 1:10,000 scale geological map of the Stardalur volcano area (after Pasquarè and Tibaldi [2007](#)); **b** N–S geological cross-section (trace A–B in **a**) of the flower structure; **c** photo of the core of the structure

their real-time monitoring allowed volcanologists to study the volcanic plumbing systems dynamically (Spaans and Hooper 2016; Woods et al. 2019; Rodríguez-Cardozo et al. 2021).

Stardalur stands on the periphery of the current Langjökull glacier, a compound of 10 outlet glaciers, the second largest ice cap in Iceland that covers at least three volcanic systems (Hodgkins et al. 2013). The Langjökull glacier has experienced glacier surging and ice-front calving during the last 400 years, having a new maximum Neoglacial extent in the Little Ice Age (two peaks around 1840 and 1890, respectively) and began its initial retreat in the twentieth century (Flowers et al. 2007; Larsen et al. 2015). The probable age of emplacement of the Stardalur cone sheet-laccolith system has been ascribed to the range between 1.7 and 0.8 Ma ago (Fridleifsson 1977). Within the same time interval, Johannesson and Saemundsson (1998) suggested the occurrence of an ice cap, though its exact age has not been defined. As the precision of these time constraints does not allow us to establish if there was the superimposition of a glacial cap over the sheet laccolith-system or not, we have chosen to run our numerical models simulating both the presence and absence of an ice cap. Hence, our work aims to facilitate understanding of how a deglaciation scenario influences sill emplacement in the shallow crust and to identify whether the Stardalur flower structure was formed because of the local stresses either wholly or partly due to glacio-isostatic deformation.

Input data and methods

Field data

Field observations focus on examples of inclined sheet and dyke-sill transitions. The first is represented by the rotation of inclined sheets gradually transitioning into horizontal sills (Fig. 3a), thus resulting in a convex-upward geometry. It is worth noting that gradually rotating sheets represent the most common type of transition observed. The second type of transition is the abrupt transition of a lower, vertical feeder dyke into an upper, horizontal sill (Fig. 3b), which was observed less frequently. Considering the field data from Tibaldi and Pasquaré (2008), the studied dykes have a thickness in the range of 1–8 m.

At the time of emplacement of these intrusion complexes, the crustal overburden was 1.5–2 km thicker (Gudmundsson 1998) and was successively partially eroded. The tectonic stress regime in the Esja area was complicated by the presence of both normal and strike-slip faults (Villemin et al. 1994; Tibaldi et al. 2008) and the existence of transcurrent faulting in adjacent areas (Bergerat et al. 1990; Passerini et al. 1997; Tibaldi et al. 2013).

The combination of centrally dipping sheets towards a shallow intrusion made of sills stacked atop each other was termed a 'flower intrusive structure' (Tibaldi and Pasquaré 2008) (Fig. 2c). This structure is observed elsewhere in Iceland in the form of shallow intrusive bodies (dykes

Fig. 3 **a** Non-annotated Fig. 3c, **b** non-annotated Fig. 3d, **c** an inclined sheet gradually rotating into a horizontal sill; this geometry has been commonly observed in sheets, which are not offset by any other intrusions; **d** a dyke is abruptly deflected into a horizontal sill; this geometry has been observed less frequently. Modified from Tibaldi and Pasquaré (2008)
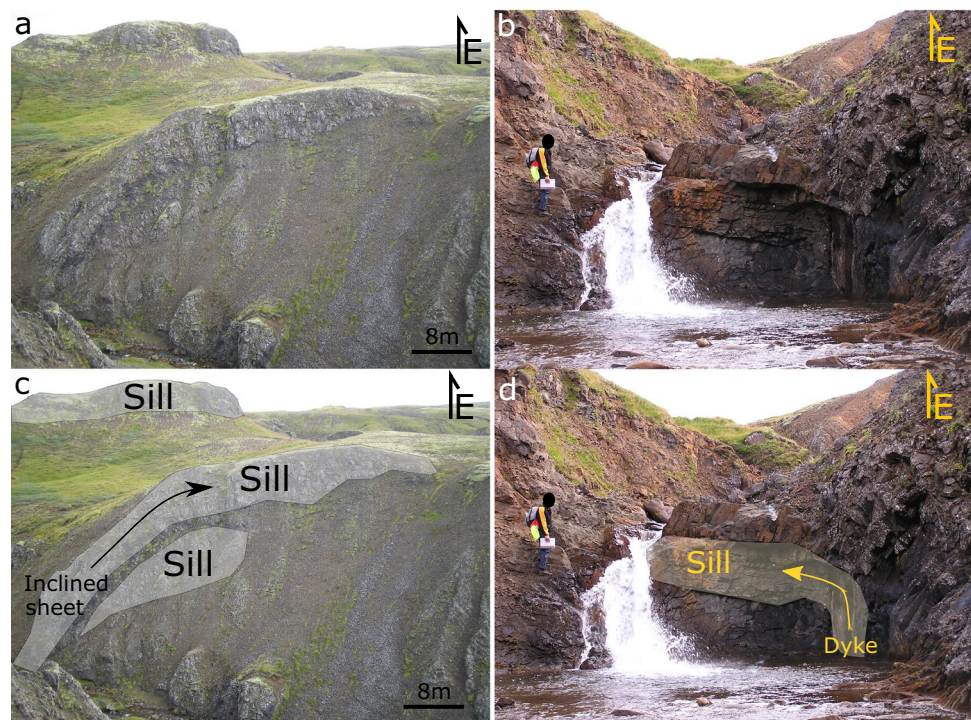
and inclined sheets) in the lowermost portions of eroded volcanoes.

The Stardalur laccolith is an outstanding example of inclined sheets and dyke-sill transitions, but it is not unique; therefore, understanding the mechanism that controlled its emplacement is fundamental. In the Esja peninsula in south-western Iceland, Tibaldi et al. (2008) described the presence of another 'flower intrusive structure' in the Thverfell magmatic complex. In eastern Iceland, Pasquaré Mariotto and Bonali (2021) documented a dyke feeding a succession of gently inclined sills, stacked atop each other, and forming a half-flower intrusive structure, similar, although much smaller, to the structure documented by Tibaldi and Pasquaré (2008). The well-exposed basaltic Njarðvik sill in Eastern Iceland is another example of a sharp inclined sheet-stacked sill transition. The sill is composed of at least seven units emplaced at a mechanical interface between basalts (top) and rhyolites (bottom) (Burchardt 2008; Burchardt et al. 2022). Similar inclined sheets/dykes to sill transitions have been found in other places around the globe. In Elba Island (Italy), Westerman et al. (2015) reported sills forming a multi-sheet intrusive complex accompanied by magmatic and magnetic textures indicative of the geometry of the feeding system. In NW Scotland, Mathieu et al. (2015) and Magee et al., (2012) studied a system of transgressive inclined sheets to sills and back to cone-sheet transitions in the Ardnamurchan sub-volcanic complex that interact with a mechanically layered crust of metasedimentary country rocks. In the Isle of Mull, Scotland, Stephens et al. (2017) also reported inclined sheet-sill transitions in Loch Scridain Sill Complex. Finally, in the Faroe Islands, Walker (2016) documented the transgressive geometry of the Streymoy sill in mechanically layered units composed of multiple lavas.

All the above show that the Stardalur laccolith bears a representative geometry of dyke to sill feeding transitions (Galland et al. 2018); hence, our modelling results can be universally applied to other areas and shall explore how similar geometries are mechanically possible in different stress fields, including glacier retreat.

Finite element method (FEM) analysis

We designed FEM (models using the structural module of the software COMSOL Multiphysics® (v5.6) (www.comsol.com. COMSOL AB, Stockholm, Sweden). The software allows us to simulate elastic deformation in 2D as well as the accumulation and distribution of stresses and strains around dykes subject to user-defined loading conditions. COMSOL permits the simulation of heterogeneous domains and allows us to incorporate distinct materials with dissimilar mechanical properties into our analyses.

To answer our key research questions, we have designed the following four boundary conditions, which we applied progressively in the models. In the beginning, we study the effects of each boundary load separately, and in the end, we combine them all together for our final models.

1) An overpressure (P_o) boundary load

The dyke (extensional fracture) is modelled as a cavity with a pressure boundary load applied at its margins based on the following equation (Eq. 1):

$$P = \frac{F_A}{n} \tag{1}$$

where P is the pressure acting normal on the surface in Pa, F_A is the force per unit area in N/m^2, and n is the normal to the undeformed midsurface plane. The studied dykes have a thickness in the range of 1–8 m (Tibaldi and Pasquaré 2008); no further quantitative data were available. The estimated overpressure for a 4 m (average thickness value) dyke when the Young's modulus of the crust is 5 GPa (Gudmundsson 2011) based on analytical solutions (Drymoni et al. 2020) is approximately 30 MPa. Based on in situ tensile strength calculations of crustal rocks (Amadei and Stephansson 1997; Zoback 2010), the magmatic excess pressure can be between 0.5 and 9 MPa, while the highest tensile strengths on small rock samples calculated by in situ tensile strength and laboratory analysis are close to 30 MPa (Carmichael 1989; Gudmundsson 2011 and references therein, Gudmundsson 2012). Previous field studies in Iceland (Gudmundsson 1986) and Santorini (Drymoni et al. 2020) showed that local and regional dyke overpressure values based on dyke aperture measurements are commonly 1–6 MPa. Here, we used a range of values ($P_o = 1$–30 MPa) to explore the two end-members and how different magma overpressures and varied dyke apertures, as seen in our case study, could have influenced the formation of the laccolith.

2) A thin elastic layer boundary load

Sill formation occurs via three mechanical processes, namely, (1) stress barrier due to dissimilar host rock mechanical properties, (2) elastic mismatch due to layering, and (3) Cook-Gordon debonding and delamination due to the presence of a weak mechanically dissimilar contact (Gudmundsson 2011). We designed a soft mechanical contact with material properties equal to $E_C = 0.001$ GPa, $\rho_C = 2000$ kg/m^3 and $v = 0.25$ between the lava and the hyaloclastite. The contact had a very low tensile and shear strength and could progressively delaminate allowing us to study the Cook-Gordon mechanism (Cook and Gordon 1964) and especially the formation of a sill but not the sill to laccolith transition. For the thin elastic layer tool, we applied elastic conditions at the downside part of

the boundary (contact). Equation 2 gives the total force per length as a function of extension (F_L) in N/m:

$$F_L = -k_A d(U_U - U_d - U_o) \qquad (2)$$

where k_A is the spring constant per unit area in N/(mm)^2 as seen in Eq. 3 which was computed by the material properties of the contact given by Eqs. 4–6, d is the predeformation, u_u and u_d are the displacements of the top and bottom boundary, respectively, u_o is an optional predeformation offset that indicates the stress-free conditions for the spring. This is explained in the Structural's module User's guide, v6.0 (p. 975–977).

$$k_A = k_n n \otimes n + k_s(E_3 - n \otimes n) \qquad (3)$$

$$k_n = \frac{E(1-v)}{d_s(1+v)(1-2v)} \qquad (4)$$

$$k_s = \frac{G}{d_s} \qquad (5)$$

$$v = \frac{E}{2G} - 1 \qquad (6)$$

where k_n is the normal stiffness in Pa which as seen in Eq. 4 was computed by the material properties of the contact, k_s is the bulk modulus in Pa, E is the Young's modulus (elastic modulus) in Pa, d_s is the thickness of the layer in meters, G is the shear modulus in Pa, and v the Poisson's ratio.

3) A pressure boundary load

We added a pressure boundary load at the contact between the surface and the hypothetical ice cap that mimics the vertical (planar) normal effective pressure (force per unit area) imposed to the crust by the presence (weight) of a glacier (Fig. 1a) based on Eq. 7. In our models, we explore the thinning of the glacier. The basal sliding and calving at the glacier's rims are not considered (Pfeffer 2007), and the ice dynamics and changes in the ice geometry (Poinar et al. 2015) are ignored.

$$N = P_i - P_w \qquad (7)$$

Subject to the glacier being in a frozen state (no meltwater), water pressure is zero; hence, Eq. 7 becomes (Eq. 8)

$$N = \rho g H \qquad (8)$$

where ρ is the density of frozen ice, which is equal to 0.917 g /cm^3; g is the acceleration of gravity (9.81 m/s^2); and H is the thickness of the glacier in meters. Based on Eq. 8 for a(n) (ice) cap thickness of $C_t = 1$ km, we consider a vertical load

equal to 9 MPa; for a $C_t = 580$ m, a vertical load of 5.2 MPa; and for a $C_t = 100$ m, the vertical load is restricted to 1 MPa. Although surface deformation analyses (Argus et al. 1999) in Fennoscandia and North America show that horizontal strains induced by crustal rebound have a maximum at the borders of the ice cap, still the maximum vertical movement is found at the central and thicker part of the cap (Stewart et al. 2000). Since our models do not study ice thickness variations between the cores and the rims of the glacier, we apply a constant vertical load along the whole ice cap contact. The same applies for the horizontal loads as seen below.

4) A horizontal boundary load (F_e)

The area before the glaciation experiences extension due to tectonic plate motion (Schilling 1973; Gudmundsson 1986) which is overprinted during glacial loading and decompression (glacier unloading) (Stewart et al. 2000) (Fig. 1b). During glacial unloading, the isostatic adjustment due to glacier shrinking builds up stresses at the ice cap margins (Peltier 1998). Similarly, in the shallow crust, glacial stresses due to the imposed vertical load can reach up to several tens of MPa. For example, for a 2 km thick glacier, the local extension below the cap can reach up to 20 MPa (Stewart et al. 2000) and can exceed the regional extension values (Adams 1989).

Initially, we construct an extensional and a compressional local stress field to replicate the local stress field based on the local volcanotectonic setting and the stress field variations during the formation of the laccolith in a non-glacial environment. We use an $F_{ext} = 1$ MPa to replicate the extension due to spreading and an $F_{com} = 3$ MPa (similar to Drymoni et al. 2020) to mimic a compound compressional stress field imposed by local faulting, previous dyke-sill emplacement or higher excess pressure magma chamber values (Pasquarè and Tibaldi 2007). In the next stage, we simulate an extensional stress field to replicate the conditions induced by crustal bending during glacier unloading, which reflects the sum of the local stress field imposed by the varied glacier load. To manifest this dynamic, local, extensional regime during unloading, we apply an $F_{ext} = 10$ MPa for $C_t = 1$ km, an $F_{ext} = 5$ MPa for $C_t = 580$ m, and an $F_{ext} = 1$ MPa for $C_t = 100$ m, respectively. The aforementioned boundary loads are applied as a horizontal pressure load based on Eq. 1 on the margins of the domain.

When the rheology of the crust is elastic, unloading may produce fractures/joints, and especially after deglaciation, faults can be formed due to the stress relief by the flexural deformation of the crust (Adams 1989). Glacial isostatic adjustment observations, however, have shown that glacier unloading (long-term deformation) produces viscoelastic relaxation in the crust (Jellinek and DePaolo 2003; Latychev

et al. 2005; Geruo et al. 2013; Girona et al. 2014; Yamasaki et al. 2018). In all our models, we hypothesize an elastic crust, which unloads due to changes of the glacier's vertical load. None of that unloading is accommodated inelastically/ plastically in the models but conditionally by a local extensional stress field.

We plot (i) a 2D surface that shows the distribution of the minimum principal compressive stress (maximum tensile stress) (σ_3) between 0 and 10 MPa, three arrow surfaces that model σ_1 (red arrows), σ_2 (green arrows), and σ_3 (black arrows), and a contour surface that models the von Mises absolute (x–y plane) shear stress (τ) ahead of the dyke tip between 0 and 12 MPa, (ii) a 2D surface which shows the distribution of displacement in the domain due to dyke propagation in a scale of 1 (minimum exaggeration) in km.

Our interpretations expand on investigating the stress concentration at the dyke tip and at the lava/hyaloclastite contact as well as its potential to delaminate if the soft mechanical contact is present. We do not consider the compression below the ice cap due to the vertical load or the deformation at the surface. We also do not describe the shape of the glacier (topographic effects, percentage of melting) or its general geometry. We assume a maximum thickness in a total frozen state (zero melted water) which gradually decreases homogeneously and is the same across the glacier. No models are designed to compare the core and the margins of the ice cap. Finally, the maximum displacement accommodated by contact opening (delamination) in the models is meaningless when it comes to predicting the thickness of an actual intrusion. The geometrical parameters that influence dyke propagation during glacier unloading are studied in Part II (Drymoni et al. in review).

Field-based model setups and materials

In our study area, the Stardalur laccolith was formed at the contact between the lavas (top layer) and the hyaloclastites (bottom layer) (Fig. 2b). The area is subject to unroofing down to a maximum depth of 2 km, and the thickness of the lava is 1 km. We designed a 15 × 15 km square box based on the field observations, and we separated it into two domains. The bottom domain had a thickness of 12 km and represented the hyaloclastites, and the top one had a thickness of 3 km and represented the lavas. The thickness of the hyaloclastite is exaggerated since our models focus on the lava/ hyaloclastite mechanical contact and surface conditions but not on the deeper stratigraphy.

We designed a 1-m-thick dyke at the centre and at around 3 km depth. We kept the location of the dyke in all our models at the same arbitrary depth that is very close to the lava/ hyaloclastite contact in a position where delamination can mechanically occur (Rosakis et al. 2000). We applied a free triangular mesh to the domain with a 3.03 km maximum

element size and a 0.006 km minimum element size. We performed tests to investigate if locking the edges of the ice cap nodes caused abnormal stress concentrations at the dyke tip. We designed models with fixed ice cap edges and ice cap edges without constraints, and we tested the effect of a roller constraint. In all of the models, the displacement surface (contact opening) was not affected by any of the applied constraints. Instead, although the stress surface showed minor stress concentration around the ice cap nodes, the stress conditions ahead of the dyke tip were not affected. For that reason, we kept all the corners of the domain fixed, and in the case of the ice cap, its two node edges, to avoid any rotation effects (Geyer and Gottsmann 2010; Browning et al. 2021).

We used different material properties for the host rock lithologies based on previous catalogues suitable for volcano modelling (Gudmundsson 2011; Heap et al. 2020). Specifically, we used $E_L = 10$ GPa for the lava deposit and $E_H = 1$ GPa for the hyaloclastites. In the first models, we used the normal mechanical ratio for a stiff/soft contact ($E_{UPP}/E_{LOW} = 10/1 = 10$) (Fig. 4a). Then, we mimicked a very soft contact and applied a thin elastic layer load on it with the following configurations: (1) a very soft 10 m thick (d_s) contact with stiffness (E_c) equal to 0.001 GPa and (2) a shear modulus (G) equal to 2 MPa (Fig. 4b).

Glacier studies in Iceland have estimated the maximum (1 km) and average (500 m) glacier thickness based on satellite data and in situ field studies (Rabatel et al. 2018). We modelled three glacier thickness scenarios for (i) $C_t = 1$ km replicating a hypothetical maximum thickness of the Langjokull glacier in the Little Ice Age, (ii) $C_t = 580$ m modelling its present condition (Björnsson et al. 2006), and (iii) $C_t = 100$ m mimicking a future scenario (Fig. 4c) (Table 1).

Results

Model results with no ice cap

We chose to model the dyke tip 0.5 km away from the contact to allow comparisons between the stress barrier and the Cook-Gordon mechanism. In Fig. 5a, the tensile stress mostly accumulated at the stiffer lava layer and less so at the soft hyaloclastite deposit. The shear stress concentrated around the dyke tip and crosscut the dissimilar mechanical contact. We observed σ_3 stress rotations ahead of the dyke tip and at the mechanical contact, which could imply that the dyke would become arrested or deflected at this point.

In contrast, in Fig. 5b, the contact was very soft (an elastic thin layer load is applied), and as a result, the accumulation of tensile stress in the lava layer was lower. The shear stress concentrated ahead of the dyke tip but did not crosscut the contact; instead, it was suppressed by the contact. An area with low tensile stress concentration occurred between
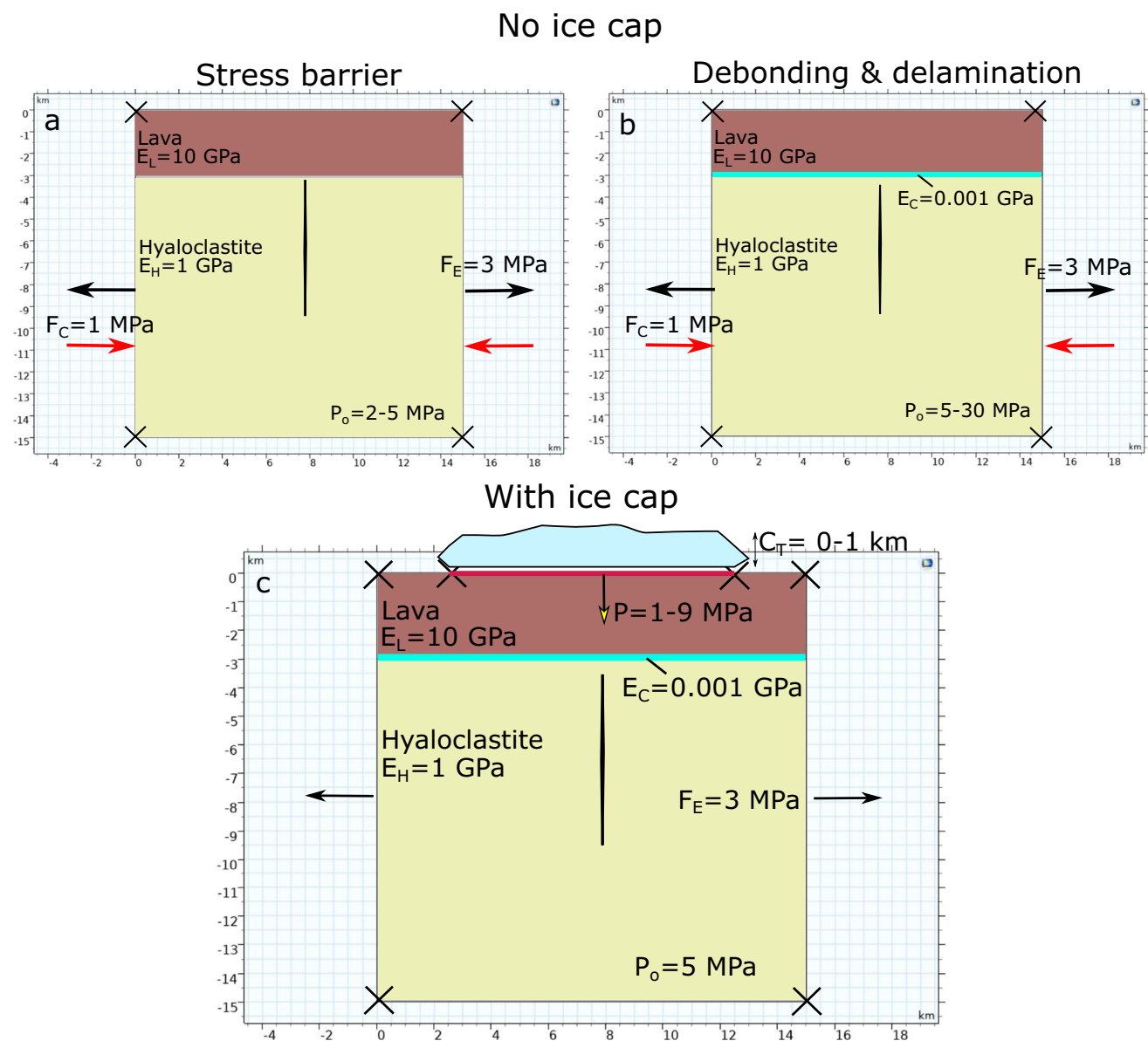
Fig. 4 Schematic illustrations of the simplified setups modelling **a** the local stress field without the ice cap, **b** delamination without the ice cap, **c** delamination with the ice cap. The red line in **c** shows the horizontal area (km) where the vertical (planar) load that mimics the ice cap has been applied in our models. The geometry and size of the glacier serves its graphical representation and bears no impact on the model

the tip and the soft contact where the latter delaminated (opened) without exhibiting stress rotations (Fig. 5b). Both of the models in Fig. 5 had the same 5 MPa overpressure in the dyke.

We ran a suite of models to explore individually the stress barrier mechanism in the domain. For this purpose, we moved the dyke tip closer to the contact (0.05 km). We tested two different overpressure values (2 MPa and 5 MPa) as well as three different boundary conditions which were an overpressure load ($P_o = 2$ MPa or 5 MPa) (Figs. 6a, d), overpressure ($P_o = 2$ MPa or 5 MPa) and horizontal extension ($F_{ext} = 1$ MPa)

loads (Figs. 6b, e), and finally overpressure ($P_o = 2$ MPa or 5 MPa) and horizontal compression ($F_{com} = 3$ MPa) loads (Figs. 6c, f). The results are shown in Fig. 6.

In models 'a' and 'b', we applied a 2 MPa and 5 MPa overpressure load, respectively. We observed that in both models, the tensile stress is mostly concentrated at the stiff lava layer and less so at the soft hyaloclastite deposit. Similarly, the shear stress in Fig. 6a developed only at the soft deposit. When we increased the dyke's overpressure (Fig. 6b), the tensile stress increased proportionally, and the shear stress was distributed equally in the domain and in the

Table 1 A summary of all the different models presented in this study. The blue-shaded models represent tensile and shear stress surfaces, while the yellow-shaded models represent displacement surfaces

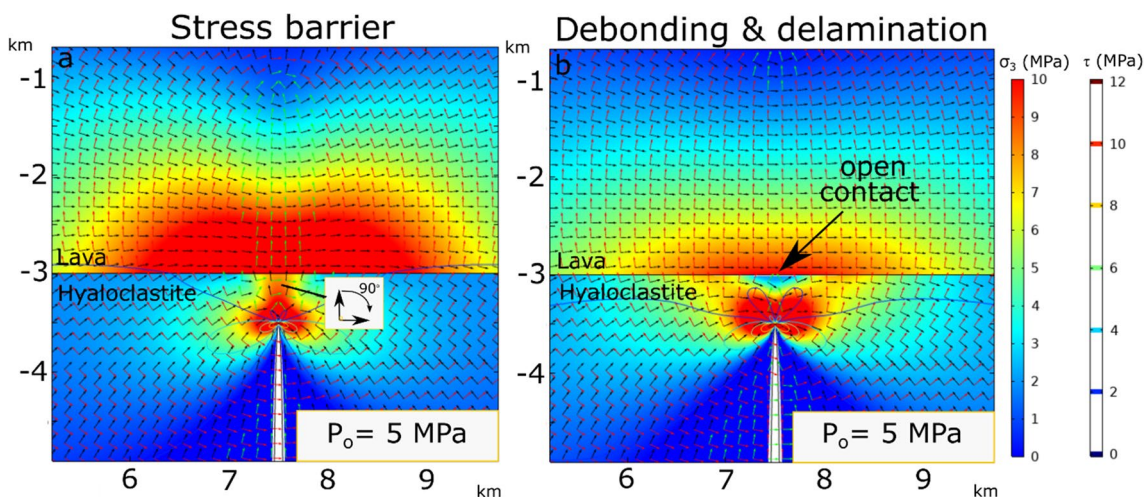|	Models	
	No Ice cap	With Ice cap
Boundary loads and studied parameters	1. Stress barrier (normal contact) Vs Debonding & delamination (weak contact) (Fig. 5)	1. A thinning ice cap (normal contact, weak contact, normal contact + F_{ext}, weak contact + F_{ext}) (Fig. 9)
	2. Stress barrier (P_o, $P_o + F_{ext}$, $P_o + F_{com}$) (Fig. 6)	2. A thinning ice cap (normal contact, weak contact, normal contact + F_{ext}, weak contact + F_{ext}) (Fig. 10)
	3. Debonding & delamination (increasing P_o) (Fig. 7)	
	4. Debonding & delamination (P_o, $P_o + F_{ext}$, $P_o + F_{com}$) (Fig. 8)	

Fig. 5 COMSOL snapshots of a 5 MPa dyke ahead of a lava/hyaloclastite contact showing the tensile stress (σ_3) as a surface distribution and the shear stress (τ) as contours around the dyke tips. **a** Simplified model (normal mechanical contact) based on Fig. 4a setup. **b** Sim-plified model (elastic thin layer contact) based on Fig. 4b setup. The arrow surface shows σ_1 (red arrows), σ_2 (green arrows), and σ_3 (black arrows)

lava layer above. In both models, stress rotations occurred inside the hyaloclastite layer; hence, the dyke would be likely to arrest or deflect at the contact.

In the next model runs (Fig. 6c, d), we applied two boundary loads (overpressure and horizontal extension) to replicate the stress field in extensional regimes such as in Iceland. The models showed similar patterns with the previous runs (Fig. 6 a, b); the extensional domain increased the tensile and shear stress concentration around the tip, and stress rotations formed at the contact. In the

final run, we applied an overpressure load coupled with a horizontal compression. With lower overpressure values (Fig. 6e), the dyke was unlikely to propagate higher in the succession because stress rotations occurred in the lava layer. However, with higher overpressure values (Fig. 6f), stress rotations appeared in both the lava and hyaloclastite layers. The dyke in Fig. 6e could propagate and crosscut the contact, but it may be arrested or deflected into the lava layer. However, in Fig. 6f, the dyke could change into a sill at the contact.
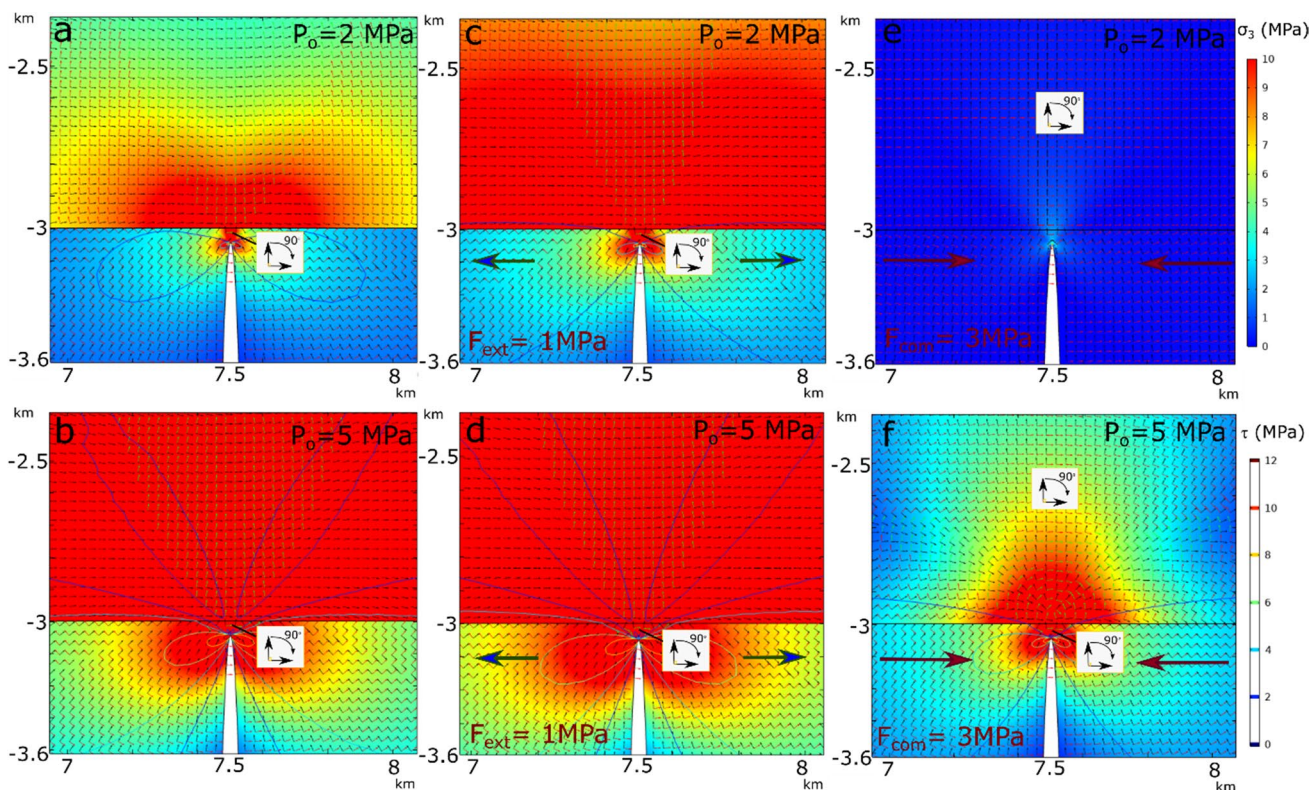
Fig. 6 COMSOL models (based on Fig. 4a simplified setup) showing the tensile stress ($\sigma 3$) as a surface distribution and the shear stress (τ) as contours around the dyke tips for different sets of boundary load-ing conditions (overpressure (**a**, **b**), overpressure and extension (**c**, **d**), overpressure and compression (**e**, **f**)). The arrow surface shows σ_1 (red arrows), σ_2 (green arrows), and σ_3 (black arrows)

In the next model runs, we increased the overpressure of the magma and added a thin elastic layer boundary load to explore the effect of the Cook-Gordon debonding and delamination mechanism in the domain. We moved the tip of the dyke to its original selected position (as seen in Fig. 5). In Fig. 7a, the overpressure was very low ($P_o = 1$ MPa), so no stress concentration or opening (very low tensile stress

concentration) was observed at the very soft contact. Similarly, no 90° stress rotations occurred at the dyke tip or at its vicinity. When we increased the overpressure to 15 MPa (Fig. 7b), then the tensile and shear stresses accumulated around the tip and the contact could delaminate. When we increased the magma overpressure to 30 MPa (Fig. 7c) mod-elling the mean value of the observed thickness range in the
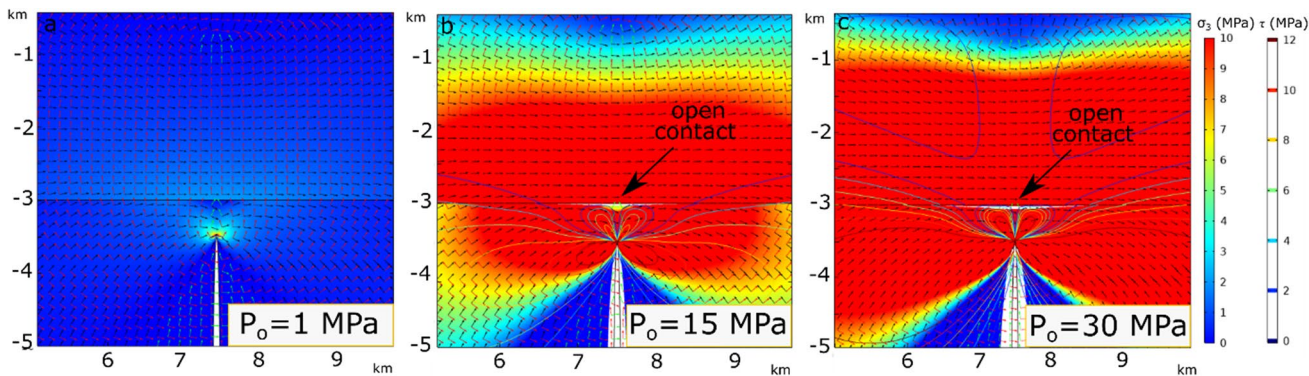

Fig. 7 COMSOL snapshots of a dyke close to a very soft (thin elas-tic layer) lava/hyaloclastite contact showing the tensile stress (σ_3) as a surface distribution and the shear stress (τ) as contours around the

dyke tips for varying values of overpressure. The arrow surface shows σ_1 (red arrows), σ_2 (green arrows), and σ_3 (black arrows)

field (4 m thickness), the tensile and shear stresses were even higher, and the contact opening became wider.

To investigate in more detail the amount of delamination at the contact, we plotted the displacement surfaces of the aforementioned models (Fig. 8) for values of dyke overpressure of 5 MPa, 15 MPa, and 30 MPa, respectively. We also modelled three different boundary loading conditions similar to Fig. 6. When the overpressure was 5 MPa (Fig. 8a), higher displacement values were accommodated inside the soft hyaloclastite layer in contrast to the lava layer. In the next two models (Fig. 8b and c), we added a second load (horizontal extension or compression, respectively) to act simultaneously at the domain. The model in Fig. 8b showed that the displacement in the lava layer increased compared to Fig. 8a and the opening (delamination) at the contact was larger (slightly thicker) than before. However, when the horizontal load was compressional, almost no displacement existed in the lava layer and the contact could not delaminate.

In the next suite, we first increased the overpressure of the dyke to 15 MPa (Fig. 8d), and then we added an extensional (Fig. 8e) and a compressional stress field, respectively

(Fig. 8f). We observed that both layers accommodated the same (maximum) amount of displacement in both models. The contact delaminated clearly in both cases forming the shape of a thicker sill than in the previous runs (Fig. 8a and b). In the next model of this suite (Fig. 8f), low to medium values of displacement existed in the lava layer above the dyke tip, but here, the contact slightly delaminated accommodating lower displacement values.

Finally, we increased the overpressure of the dyke to 30 MPa. The models showed the conditions that favour thicker sill formation (no width changes were observed). Since here we are only interested in exploring the mechanism that formed the Stardalur laccolith and not its geometry and mechanical evolution, we expand those aspects in Part II (Drymoni et al. in review).

Model results with an ice cap

In the next model suites, we hypothesise the existence of an ice cap resting on top of the domain (Fig. 4c). We examine how the variable glacier thickness (vertical load)
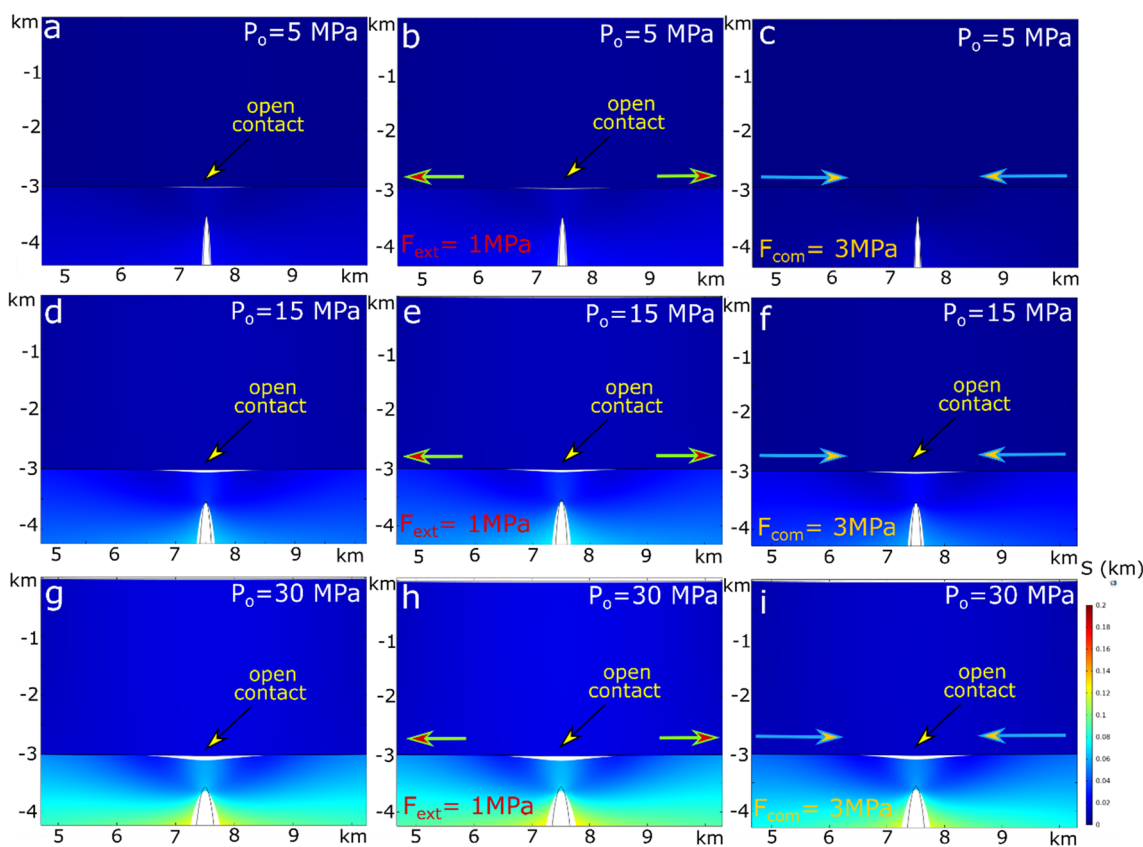

Fig. 8 Displacement surfaces at the very soft contact (elastic thin layer) subject to increasing values of dyke overpressure and combinations of boundary loading conditions, i.e., dyke overpressure (**a, d,** **g**), dyke overpressure and local extension (**b, e, h**), dyke overpressure and local compression (**c, f, i**)
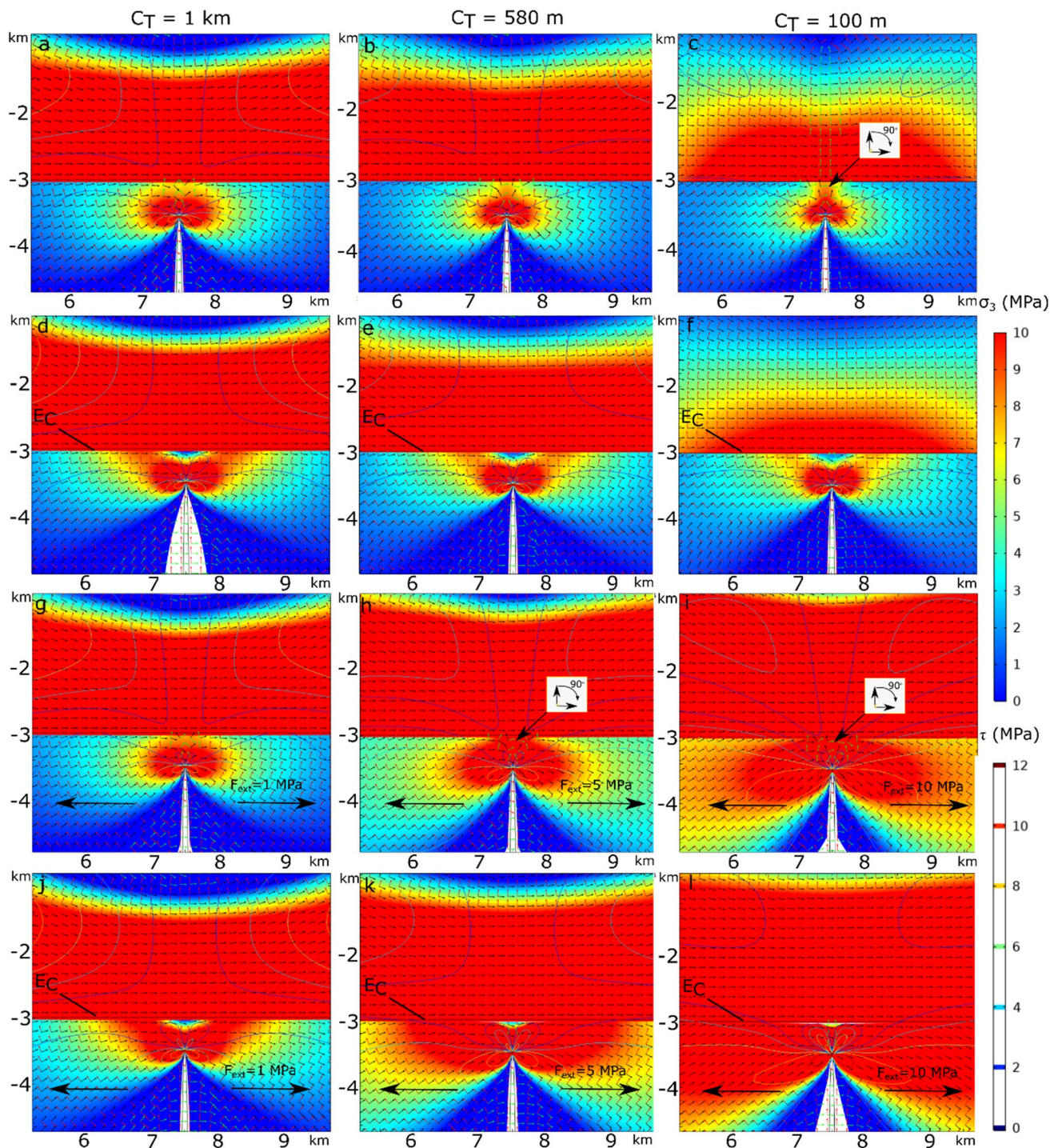
Fig. 9 COMSOL models showing the tensile (σ_3) (filled contours) and shear (τ) (line contours) stresses around a dyke that approaches a normal lava/hyaloclastite contact (**a–c**, **g–i**) and a very soft (thin elastic layer) contact (Ec) (**d–f**, **j–l**) subject to variable vertical load (glacier thickness (0.1–1 km)) and crust extension (**g–l**). The overpressure of the dyke is always 5 MPa, the location of the dyke tip is constant, the red arrows show σ_1, the green arrows show σ_2, and the black arrows show σ_3. All the models include the glacial effect

affects the dyke propagation paths in the shallow crust and possibly the emplacement of the Stardalur laccolith. We modelled four scenarios, which are shown in Figs. 8 and 9:

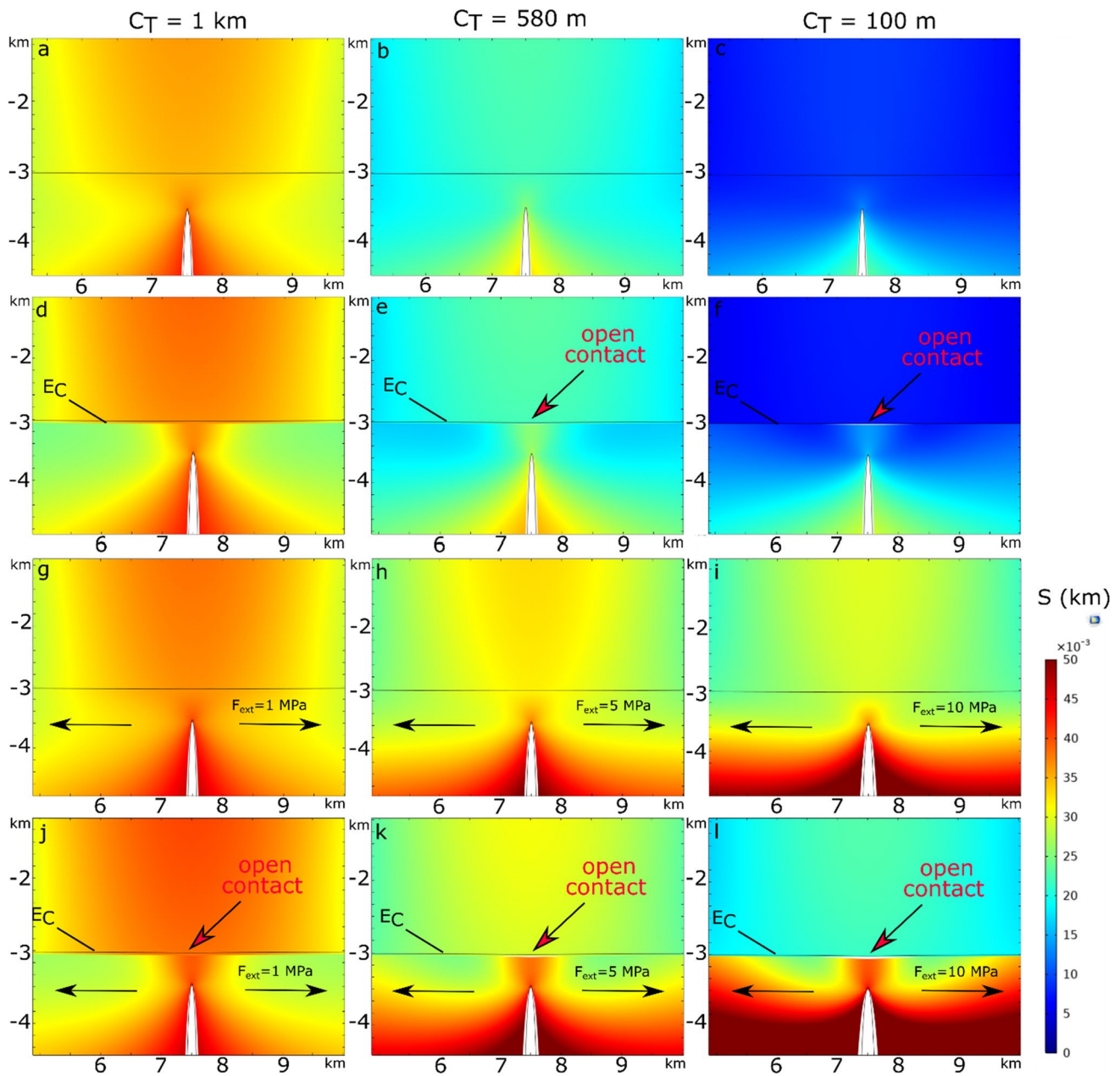i. The effect of a glacier with variable thickness (1–9 MPa vertical load) in a layered crust (Fig. 9a–c and 10a–c).

Fig. 10 COMSOL models showing the deformation around a dyke that approaches a simple lava/hyaloclastite contact (**a–c, g–i**) and a very soft (thin elastic layer) contact (**d–f, j–l**) subject to variable vertical load (glacier thickness (0.1–1 km)) and crust extension (**g–l**). The overpressure of the dyke is always 5 MPa, and the location of the tip remains constant. All the models include the glacial effect

ii. The effect of a glacier with variable thickness (1–9 MPa vertical load) in a layered crust that accommodates a thin elastic layer boundary contact (Fig. 9d–f and 10d–f).

iii. The effect of a glacier with variable thickness (1–9 MPa vertical load) in a layered crust subject to a local extensional regime (F_{ext} = 3 MPa) (Figs. 9g–i and 10g–i).

iv. ii.The effect of a glacier with variable thickness (1–9 MPa vertical load) in a layered crust that accom-

modates a thin elastic layer boundary contact subject to a local extensional regime (F_{ext} = 3 MPa) (Figs. 9j–l and 10j–l).

In the first scenario, we simulated a vertical load of 9 MPa (Fig. 9a) to explore the conditions of the crust when the glacier was hypothetically at its maximum thickness (C_t = 1 km) in the past. We observed a high tensile stress concentration at the dyke tip and at the lava layer and stress rotations

at the lava/hyaloclastite contact, which did not reach more than 45°. The shear stress was distributed through the whole domain and approached the surface. In the next run, we reduced the thickness of the glacier ($C_t = 580$ m) (vertical load of 5 MPa) to replicate its present state (Fig. 9b). We observed almost 90° stress rotations at the lava/hyaloclastite contact. The tensile stress showed higher concentrations close to the contact and in the lava layer, whereas the shear stress followed similar patterns as in Fig. 9a. Finally, we reduced the thickness of the glacier to $C_t = 100$ m (vertical load of 1 MPa) to address the dyking conditions in a future scenario (Fig. 9c). The model showed 90° stress rotations at the lava/hyaloclastite contact and high tensile stress at the tip and its vicinity; however, the shear stress was mostly located around the tip, and very low concentrations were restricted in the middle of the lava layer.

In the next round, we modelled the same concept, but we applied an extra boundary load: a thin elastic layer at the lava/hyaloclastite contact. In the first model (Fig. 9d), where the thickness of the glacier was at its maximum, the results were similar as in Fig. 9a. High tensile stress was concentrated at the dyke tip and the lava layer, but lower concentrations occured at the very soft contact just at the front of the dyke tip. This area of stress concentration denoted the delaminated zone. No stress rotations were observed. The next model (Fig. 9e) had high tensile stress and shear stress concentration around the tip and in the lava layer, but no stress rotations were seen at the contact. Finally, the last model (Fig. 9f) showed similar tensile stress values with the previous models (Fig. 9d and e), but the shear stress was again suppressed by the very soft contact so they could not distribute at the lava layer.

In the third scenario, we added a horizontal boundary load to the first concept to replicate the unloading of the crust, which was accommodated by extension due to crustal flexure. Our results (Fig. 9g–i) showed that the application of the extensional stress field increased the concentration of tensile and shear stresses at the dyke tip and the lava layer. However, it did not alter the stress rotations at the contact, which existed when the thickness of the glacier (C_t) was 580 m (Fig. 9h) and 100 m (Fig. 9i).

In the last scenario, we explored how the existence of an extensional stress field could affect the formation of a laccolith. All models (Fig. 9j–l) showed that horizontal extension increased the accumulation of tensile and shear stresses at the dyke tip and its vicinity without promoting any stress rotations at the very soft contact. Interestingly, shear stress builts up in the lava layer in all the models.

We reran the same model suites and produced 2D displacement surfaces during glacier retreat (Fig. 10) for a normal (simple mechanical ratio) (a–c, g–i) and a very soft contact (elastic thin layer) (d–f, j–l). The models showed that when the thickness of the glacier was at its minimum ($Ct = 100$ m), then the lava layer exhibited lower displacement values than the rest of the runs (Fig. 10 c, f). No displacement was observed when the dissimilar contact was modelled as a simple mechanical ratio (Fig. 10a–c). However, when the very soft contact existed, the latter delaminated and the displacement in the lava layer reached its maximum (Fig. 10d, e). Similarly, the contact opened when the thickness of the glacier was retreating (the thickness reduced from 580 to 100 m) (Fig. 10e, f). Subject to the existence of an extensional stress regime (Fig. 10g–l), the displacement gradually increased and the contact delaminated when the glacier thickness decreased (Fig. 10j, k, l). Interestingly, with or without crust extension, the opening became wider subject to less glacier load.

Discussion

Previous studies of the Stardalur laccolith in the field (Pasquarè and Tibaldi 2007) have focused mostly on its structural implications and provided insights on its possible emplacement. Field studies led to the suggestion that the formation of the observed sill-like geometries was caused by stress rotations in response to excess magma pressure in a shallow magma chamber or the effect of the heterogeneous crust (since the laccolith was emplaced at the rheological boundary between dominant upper lavas and lower hyaloclastites).

Dyke-sill transitions are often produced when the local stress field becomes compressional (Gudmundsson 1998). This can occur at the local scale due to force imposed by prior dyke injections, faulting, or graben subsidence. Similarly, stiffness contrasts and layer thickness implications can produce stress rotations at the dyke tips in heterogeneous and anisotropic segments (Drymoni et al. 2020). In particular, the propagation of a dyke from a soft to a stiff layered elastic domain can promote arrest or dyke-sill deflection (Gudmundsson and Brenner 2004; Maccaferri et al. 2010; Gudmundsson 2011; Drymoni et al. 2020). Yet, when a dyke propagates from a stiff to a soft layer, arrest is also possible at the interface with the soft layer (Forbes Inskip et al. 2020). Finally, analogue experiments have provided evidence of sill emplacement subject to compressive regional stresses (Menand 2011) and rigidity contrasts (Kavanagh et al. 2006, 2018).

What mechanical processes could have formed the Stardalur laccolith?

In this paper, we carried out a numerical study based on the previous collected field data, and our first target was to understand the mechanical processes that could have formed the Stardalur laccolith. Since its emplacement occurred in between layers of dissimilar mechanical properties, namely,

lavas and hyaloclastites, we explored two mechanisms that are responsible for dyke-sill transitions, namely, the stress barrier and the Gook-Gordon debonding and delamination.

Tensile and shear stresses are seen to accumulate at the stiff lava layer and at the vicinity of the dyke tip in all case scenarios. Stress rotations occur mostly in the soft hyaloclastite layer and at the studied contact. Since those conditions can equally promote dyke arrest and dyke-sill emplacement, we tested the existence of a very soft contact (thin elastic layer) between the lava and the hyaloclastite and its ability to delaminate. We propose that both mechanical processes could have been accountable for the formation of a sill but not for the Stardalur laccolith. This is because, based on the coupled 2D tensile stress (σ_3) and displacement surface models, lower overpressure values ($P_o \leq 5$ MPa) can promote stress rotations and, hence, can equally promote either dyke-arrest or dyke-sill deflection without contact opening. However, with higher overpressure values ($P_o > 5$ MPa), although stress rotations still occur, the contact can also open and promote theoretically larger displacements, which can accommodate the thick stacked-sill structure. Hence, our models have shown that high overpressure values ($P_o > 5$ MPa) and a thin elastic layer load are necessary for the delamination of the contact and the formation of the laccolith.

These findings are in agreement with previous studies, which investigated the emplacement of laccoliths and the formation of space accommodated by later intrusions above a sill. The 'laccolith concept' originates initially from Gilbert (1877) and Hunt (1953) and their observations in the Henry Mountains (Utah). Yet, field observations have revealed mainly two mechanisms for the formation of a laccolith: (i) sill stacking, e.g., Henry Mountains (Johnson and Pollard 1973), Axial Seamount (Carbotte et al. 2020), Elba island (Westerman et al. 2015; Farina et al. 2010), Stardalur (Tibaldi and Pasquaré 2008), (ii) magma viscosity (Mattsson et al. 2018; Burchardt et al. 2019) (due to strain-rate magma rheology) and host rock properties (Gudmundsson 2011; Schmiedel et al. 2017). In the latter, laccoliths can be formed by uplifting and flexuring the overburden when sills (repeated intrusions) gradually become thicker due to higher overpressure conditions (Acocella 2000; Turcotte and Schubert 2002). Similarly, our study has shown that the Stardalur laccolith could have formed by progressive dyke-sill transitions that occurred at the contact between a stiff and a soft layer subject to increasing dyke overpressure conditions. However, further numerical studies are needed to investigate its stacked sill geometry.

Effect of dyke overpressure, local stress field, and contact stiffness on the dyke to sill transition

We studied three different boundary loads (overpressure, overpressure with extension, overpressure with compression) to replicate the probable stress fields during laccolith emplacement. The models have shown that in the absence of the thin elastic layer, the hyaloclastite becomes a temporary stress barrier subject to the overpressure and extension loading condition. This scenario does not replicate the field observations because multiple dyke injections form compressional settings (Gudmundsson 2020). In contrast, in compressional settings, the top lava layer revokes dyke propagation and the dyke would either become arrested or deflected at the contact. The field observations instead have shown that the flower structure formed at the lava/hyaloclastite contact and the stacked sills were emplaced in the lava layer. Our models propose that subject to a compressional stress regime, stress rotations could have encouraged dyke-sill transitions (Fig. 6c, f), but still the contact cannot delaminate, although an amount of displacement is accommodated. It is hence unlikely that a 200–400 m thick laccolith may have been emplaced under those conditions.

We tested the same stress field scenarios with the existence of a thin elastic layer at the contact. The latter has the ability to delaminate and accommodates slightly higher theoretical displacements by 5% in contrast to the previous scenario where the crustal segment can also accommodate theoretical displacements but without contact opening. Not all the loading scenarios encourage stress rotations, but delamination occurs when the overpressure is higher ($P_o \geq 5$ MPa) in our models. However, in compressional regimes (Fig. 8c, f, i), delamination occurs if only the overpressure is more than 15 MPa ($P_o \geq 15$ MPa) in our models. Instead, all the models highlight that an extensional regime greatly encourages delamination, which may imply that stress barriers and Cook-Gordon delamination occur mainly in different stress conditions, namely, compression and extension, respectively.

The Stardalur laccolith was emplaced in an area dominated by an extensional regional regime associated with plate spreading (Gudmundsson 2000). At a local scale, during the laccolith's emplacement, a compressional stress field occurs due to the compressional force imposed by prior dyke injections, some of which eventually formed sills. Based on Pasquarè and Tibaldi (2007), a compressional stress field induced by the high excess magma pressure (P_e) of the shallow magma chamber is rare but also likely. Those conditions imply a local but gradually increasing compressional stress regime while the formation of the stacked-sill structure is progressing. Our numerical models are in agreement with this hypothesis; however, they suggest that for a laccolith to be formed, the dyke overpressure in every injection should be very high ($P_o \geq 15$ MPa). Yet, large displacements and contact opening can still occur in the presence of a local extensional regime, an unlikely condition according to the structural analysis.

How does unloading due to glacier thinning influence dyking in the shallow crust?

During glaciation, the shallow crust accommodates several MPa of stresses owing to the glacier vertical load. During glacier unloading, the crust accommodates an extensional stress field that can exceed the regional extension and over-prints all the previous stress regimes (Adams 1989; Stewart et al. 2000). We explored the stress accumulation around the dyke tip and at the contact (Fig. 9) below an ice cap. We examined if dyke-sill transitions are encouraged in a similar contact as the one found at Stardalur and under which loading conditions. We tested how the rebound effect due to gradually lower vertical load (glacier thickness) encouraged stress rotations for the case where a thin elastic layer is initially not applied at the contact (Fig. 9a–c). Then, we examined the delamination process when a thin elastic layer is applied at the contact subject to crust unloading (Fig. 9d–f). Our models have shown that stress rotations occur in the hyaloclastite layer and at the lava/hyaloclastite contact when the glacier thickness decreases. The presence of an extensional stress field when the contact is normal shows similar results (Fig. 9g–i). However, when in the same loading conditions the thin elastic layer is applied to the contact, stress rotations occur neither at the hyaloclastite nor at the contact (Fig. 9j–l).

Finally, we investigated the displacement accommodated at the contact and especially how likely it is for a laccolith to form during glacier retreat. Our results show that the contact cannot delaminate without the thin elastic layer (Fig. 10a–c, g–i). In the opposite scenario, delamination successfully occurs when the thickness of the glacier is gradually decreasing (Fig. 10e and f), and this outcome is even more likely to occur when a horizontal extensional regime is applied at the domain (Fig. 10k and l). Yet, the existence of a moderate extensional stress field ($F_{ext} \geq 5$ MPa) encourages laccolith formation at the contact. Also, the delamination geometry shows differences between the models. In detail, the sill becomes wider when the vertical load is lower, an observation in agreement with previous analogue models that studied the influence of the overburden thickness to the geometry of the laccolith (Roman-Berdiel et al. 1995).

Normally, glacier retreat enhances the generation of magma in the shallow crust, volcanic activity, and dyking in the long term (Gudmundsson 1986; Sigvaldason et al. 1992; Jull and McKenzie 1996; Maclennan et al. 2002; Andrew and Gudmundsson 2007; Pagli and Sigmundsson 2008; Sigmundsson et al. 2010; Geyer and Bindeman 2011; Bakker et al. 2016; Sulpizio and Massaro 2017), as well as magma accumulation in the short term (Hooper et al. 2011). Our results suggest that during glacier retreat and under specific mechanical conditions, dyke-sill interactions can still occur, and magma may stall in the shallow crust. Finally, in all our models, we hypothesise an elastic crust although viscoelastic

conditions are also expected to influence the crust during long-term deglaciation (> 100 years) (Latychev et al. 2005; Girona et al. 2014; Sigmundsson et al. 2015; Yamasaki et al. 2018). We aim to explore the effects of a viscoelastic crust in a future study.

The following four general scenarios all satisfy the conditions for dyke to sill deflection possibly enhancing the formation of a laccolith in (i) non-glacial and (ii) glacial volcanotectonic settings such as that at Stardalur (Fig. 11):

1) A thin elastic layer exists, the overpressure of the dyke is low ($P_o = 2$ MPa), and low horizontal extension is applied (due to plate spreading) (Fig. 11a). This condition simulates the first dyke to sill deflection in Stardalur in a non-glacial scenario.
2) A thin elastic layer exists, the overpressure of the dyke will be very high ($P_o = 15$ MPa), and high horizontal compression is applied (due to pre-existing dyke emplacement) (Fig. 11b). This condition simulates the subsequent dyke to sill deflection in Stardalur in a non-glacial scenario.
3) A thin elastic layer exists, the overpressure of the dyke will be moderate to high ($P_o = 5$ MPa), and low horizontal extension is applied (due to unloading) (Fig. 11c). This condition simulates a dyke to sill deflection in Stardalur when a 1 km thick glacier, where low uplift and bending of the crust exists, covers the area.
4) A thin elastic layer exists, the overpressure of the dyke is moderate to high ($P_o = 5$ MPa), and a high horizontal extension is applied (due to unloading) (Fig. 11d). This condition simulates a dyke to sill deflection in Stardalur when a 100 m thick glacier, where high uplift and bending of the crust exists, covers the area.

Conclusions

The soft hyaloclastite layer may be a temporary stress barrier for an approaching dyke with a range of overpressures between 2 and 5 MPa, subject to local extension ($F_{ext} = 1$ MPa). However, in compressional regimes, similar stress barriers occur only when the dyke overpressure is greater than 5 MPa. On the contrary, the stiff lava layer may become a temporary stress barrier for an approaching dyke only when the overpressure is low ($P_o = 2$ MPa) and horizontal compression is applied to the domain. Yet, the existence of a very soft contact (thin elastic layer) between the lavas and the hyaloclastites suppresses the distribution of shear stress towards the surface.

The conditions of contact opening (delamination) are not met when the overpressure is low ($P_o = 5$ MPa) in a compressional domain. Delamination in compressional regimes occurs if only the overpressure is more than 5 MPa
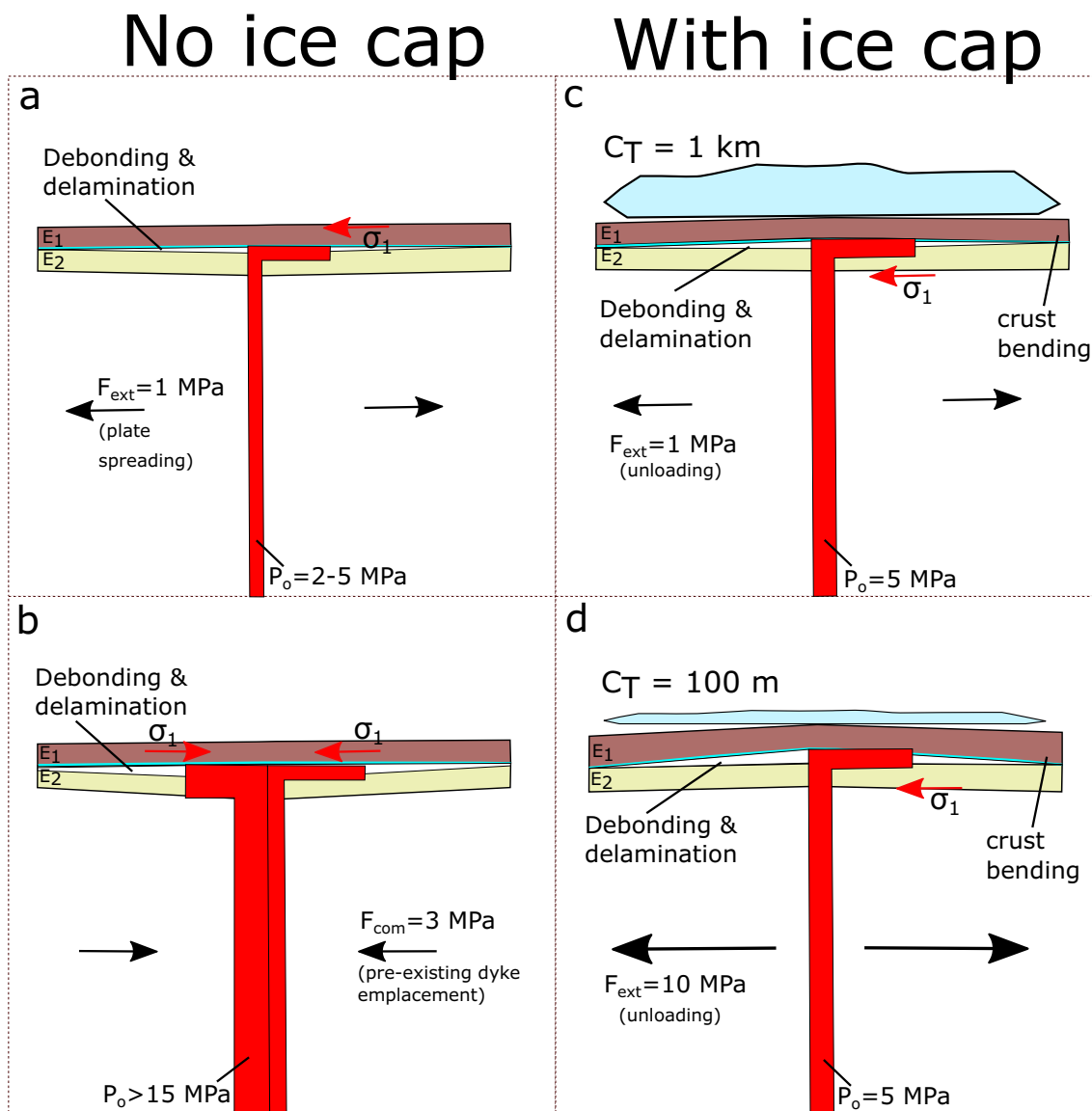
Fig. 11 Schematic illustration showing the mechanical conditions (scenarios) that promote dyke-sill transitions in volcanotectonic settings without a glacier (**a**, **b**) and with a glacier (**c**, **d**). The geometry of the glacier in **c** and **d** serves its graphical representation and bears no impact on the models

($P_o \geq 5$ MPa). Extensional regimes encourage delamination at the contact but also higher concentration of tensile and shear stresses in the stiff layer and in the vicinity of the tip. Finally, the extension due to crust flexure makes the delamination wider and thicker when the vertical load (glacier thickness) is lower.

Author contribution Conceptualization: Kyriaki Drymoni; formal analysis and investigation: Kyriaki Drymoni; visualization: Kyriaki Drymoni; writing–original draft preparation: Kyriaki Drymoni; conceptualization of field data: Alessandro Tibaldi, Federico Pasquare Mariotto; review and editing: Kyriaki Drymoni, Alessandro Tibaldi, Federico Pasquare Mariotto, Fabio Luca Bonali.

References

Acocella V (2000) Space accommodation by roof lifting during pluton emplacement at Amiata (Italy). Terra Nova 12:149–155

Acocella V (2021) Volcano-tectonic processes. Springer Nature

Adams J (1989) Crustal stresses in eastern Canada. In Earthquakes at North-Atlantic passive margins: neotectonics and postglacial rebound. Springer, Dordrecht

Ágústsdóttir T, Woods J, Greenfield T, Green RG et al (2016) Strikeslip faulting during the 2014 Bárðarbunga-Holuhraun dike intrusion, central Iceland. Geophys Res Lett 43:1495–1503

Albino F, Pinel V, Sigmundsson F (2010) Influence of surface load variations on eruption likelihood: application to two Icelandic subglacial volcanoes, Grímsvötn and Katla. Geophys J Int 181:1510–1524

Allen CC (1980) Icelandic subglacial volcanism: thermal and physical studies. J Geol 88:108–117

Amadei B, Stephansson O (1997) Rock stress and its measurement. Springer Science & Business Media

Andrew RE, Gudmundsson A (2007) Distribution, structure, and formation of Holocene lava shields in Iceland. J Volcanol Geoth Res 168:137–154

Argus DF, Peltier WR, Watkins MM (1999) Glacial isostatic adjustment observed using very long baseline interferometry and satellite laser ranging geodesy. Journal of Geophysical Research: Solid Earth 104:29077–29093

Arvidsson R (1996) Fennoscandian earthquakes: whole crustal rupturing related to postglacial rebound. Science 274:744–746

Bakker RR, Frehner M, Lupi M (2016) How temperature-dependent elasticity alters host rock/magmatic reservoir models: a case study on the effects of ice-cap unloading on shallow volcanic systems. Earth Planet Sci Lett 456:16–25

Bergerat F, Angelier J, Villemin T (1990) Fault systems and stress patterns on emerged oceanic ridges: a case study in Iceland. Tectonophysics 179:183–197

Björnsson A (1985) Dynamics of crustal rifting in NE Iceland. J Geophys Res: Solid Earth 90:10151–10162

Björnsson H, Guðmundsson S, Jóhannesson T, Pálsson F, Aðalgeirsdóttir G, Haraldsson HH (2006) Geometry, mass balance and climate change response of Langjökull ice cap, Iceland. The International Arctic Science Committee (IASC), Working Group on Artic Glaciology

Bovis MJ (1990) Rock-slope deformation at Affliction Creek, southern Coast Mountains, British Columbia. Can J Earth Sci 27:243–254

Browning J, Gudmundsson A (2015) Caldera faults capture and deflect inclined sheets: an alternative mechanism of ring dike formation. Bull Volcanol 77:4

Browning J, Gudmundsson A (2015b) Surface displacements resulting from magma-chamber roof subsidence, with application to the 2014–2015 Bardarbunga-Holuhraun volcanotectonic episode in Iceland. J Volcanol Geoth Res 308:82–98

Browning J, Karaoğlu Ö, Bayer Ö, Turgay MB, Acocella V (2021) Stress fields around magma chambers influenced by elastic thermo-mechanical deformation: implications for forecasting chamber failure. Bull Volcanol 83:1–13

Burchardt S (2008) New insights into the mechanics of sill emplacement provided by field observations of the Njardvik Sill, Northeast Iceland. J Volcanol Geoth Res 173:280–288

Burchardt S (2018) Volcanic and igneous plumbing systems: understanding magma transport, storage, and evolution in the earth's crust. Elsevier

Burchardt S, Mattsson T, Palma JO et al (2019) Progressive growth of the Cerro Bayo cryptodome, Chachahuén volcano, Argentina—Implications for viscous magma emplacement. J Geophys Res: Solid Earth 124:7934–7961

Burchardt S, Óskarsson BV, Gustafsson LE, Berg SE, Riishuus MS (2022) Geology of a Neogene caldera cluster in the Borgarfjörður eystri – Loðmundarfjörður area, Northeast Iceland. Volcanica 5:133–161

Carbotte SM, Arnulf A, Spiegelman M et al (2020) Stacked sills forming a deep melt-mush feeder conduit beneath Axial Seamount. Geology 48:693–697

Caricchi L, Townsend M, Rivalta E, Namiki A (2021) The build-up and triggers of volcanic eruptions. Nature Reviews Earth & Environment 2:458–476

Carmichael RS (1989) Practical handbook of physical properties of rocks and minerals. CRC Press

Cashman KV, Sparks RSJ, Blundy JD (2017) Vertically extensive and unstable magmatic systems: a unified view of igneous processes. Science 355:6331 eaag3055

Clunes M, Browning J, Marquardt C, Cortez J, Drymoni K, Kavanagh J (2023) Inclination and heterogeneity of layered geological sequences influence dike-induced ground deformation. Geology 51:278–283

Cook J, Gordon JE (1964) A mechanism for the control of crack propagation in all-brittle systems Proceedings of the Royal Society, 282:1364-5021

Cossart E, Braucher R, Fort M, Bourlès DL, Carcaillet J (2008) Slope instability in relation to glacial debuttressing in alpine areas (Upper Durance catchment, southeastern France): evidence from field data and 10Be cosmic ray exposure ages. Geomorphology 95:3–26

Dering GM, Micklethwaite S, Cruden AR, Barnes SJ, Fiorentini ML (2019) Evidence for dyke-parallel shear during syn-intrusion fracturing. Earth Planet Sci Lett 507:119–130

Douglas BC (1997) Global sea level rise: a redetermination Surv. Geophys 18:279–292

Drymoni K, Browning J, Gudmundsson A (2020) Dyke-arrest scenarios in extensional regimes: insights from field observations and numerical models, Santorini, Greece. J Volcanol Geoth Res 396:106854

Drymoni K, Browning J, Gudmundsson A (2021) Volcanotectonic interactions between inclined sheets, dykes, and faults at the Santorini Volcano, Greece. J Volcanol Geoth Res 416:107294

Drymoni K, Browning J, Gudmundsson A (2022) Spatial and temporal volcanotectonic evolution of Santorini volcano, Greece. Bull Volcanol 84:1–18

Drymoni K, Russo E, Tibaldi A, Corti N, Bonali F, Mariotto FP (2023) Dyke-induced graben formation in a heterogeneous succession on Mt. Etna: insights from field observations and FEM numerical models. J Volcanol Geother Res 433:107712

Drymoni K (2020) Dyke propagation paths: the movement of magma from the source to the surface (Doctoral dissertation, Royal Holloway, University of London)

Eberhardt E, Stead D, Coggan JS (2004) Numerical analysis of initiation and progressive failure in natural rock slopes—the 1991 Randa rockslide. Int J Rock Mech Mining Sci 41:69–87

Ebmeier SK, Andrews BJ, Araya MC, Arnold DWD, Biggs J et al (2018) Synthesis of global satellite observations of magmatic and volcanic deformation: implications for volcano monitoring & the lateral extent of magmatic domains. J Appl Volcanol 7:1–26

Eiríksson J (2008) Glaciation events in the Pliocene-Pleistocene volcanic succession of Iceland. Jökull 58:315–329

Farina F, Dini A, Innocenti F, Rocchi S, Westerman DS (2010) Rapid incremental assembly of the Monte Capanne pluton (Elba Island, Tuscany) by downward stacking of magma sheets. Bulletin, 122:1463–1479.

Fedotov SA (1981) Magma rates in feeding conduits of different volcanic centers. J Volc Geoth Res 9:379–394

Flowers GE, Björnsson H, Geirsdóttir Á, Miller GH, Clarke GK (2007) Glacier fluctuation and inferred climatology of Langjökull ice cap through the Little Ice Age. Quatern Sci Rev 26:2337–2353

Fridleifsson IB (1977) Distribution of large basaltic intrusions in the Icelandic crust and the nature of the layer 2-layer 3 boundary. Geol Soc Amer Bull 88:1689–1693

Gaffney ES, Damjanac B, Valentine GA (2007) Localization of volcanic activity: 2. Effects of pre-existing structure. Earth Planet Sci Lett 263:323–338

Galland O, Bertelsen HS, Eide CH et al (2018) Storage and transport of magma in the layered crust—formation of sills and related flat-lying intrusions. In Volcanic and igneous plumbing systems (pp. 113–138). Elsevier

Gaynor SP, Svensen HH, Polteau S, Schaltegger U (2022) Local melt contamination and global climate impact: dating the emplacement of Karoo LIP sills into organic-rich shale. Earth Planet Sci Lett 579:117371

Geirsdottir A, Eiríksson J (1994) Growth of an intermittent ice sheet in Iceland during the late Pliocene and early Pleistocene. Quat Res 42:115-130

Geruo A, Wahr J, Zhong S (2013) Computations of the viscoelastic response of a 3-D compressible Earth to surface loading: an application to Glacial Isostatic Adjustment in Antarctica and Canada. Geophys J Int 192:557–572

Geyer A, Bindeman I (2011) Glacial influence on caldera-forming eruptions. J Vol Geotherm Res 202:127–142

Geyer A, Gottsmann J (2010) The influence of mechanical stiffness on caldera deformation and implications for the 1971–1984 Rabaul uplift (Papua New Guinea). Tectonophysics 483:399–412

Gilbert GK (1877) Report on the Geology of the Henry Mountains. US Government Printing Office

Girona T, Costa F, Newhall C, Taisne B (2014) On depressurization of volcanic magma reservoirs by passive degassing. J Geophys Res: Solid Earth 119:8667–8687

Glazner AF, Manley CR, Marron JS, Rojstaczer S (1999) Fire or ice: anticorrelation of volcanism and glaciation in California over the past 800,000 years. Geophys Res Lett 26:1759–1762

Grämiger LM, Moore JR, Gischig VS, Ivy-Ochs S, Loew S (2017) Beyond debuttressing: mechanics of paraglacial rock slope damage during repeat glacial cycles. J Geophys Res Earth Surf 122:1004–1036

Grapenthin R, Sigmundsson F, Geirsson H, Árnadóttir T, Pinel V (2006) Icelandic rhythmics: annual modulation of land elevation and plate spreading by snow load. Geophys Res Lett 33:L24305

Grönvold K, Jóhannesson H (1984) Eruption in Grímsvötn: course of events and chemical studies of the tephra. Jökull 34:1–11

Gudmundsson A (1984) Formation of dykes, feeder-dykes, and the intrusion of dykes from magma chambers. Bullet Volcanol 47:537–550

Gudmundsson A (1986) Mechanical aspects of postglacial volcanism and tectonics of the Reykjanes Peninsula, southwest Iceland. J Geophys Res: Solid Earth 91:12711–12721

Gudmundsson A (1998) Magma chambers modeled as cavities explain the formation of rift zone central volcanoes and their eruption and intrusion statistics. J Geophys Res 103:7401–7412

Gudmundsson A (1999) Postglacial crustal doming, stresses and fracture formation with application to Norway. Tectonophysics 307:407–419

Gudmundsson A (2000) Dynamics of volcanic systems in Iceland: example of tectonism and volcanism at juxtaposed hot spot and mid-ocean ridge systems. Annu Rev Earth Planet Sci 28:107–140

Gudmundsson A (2006) How local stresses control magma-chamber ruptures, dyke injections, and eruptions in composite volcanoes. Earth Sci Rev 79:1–31

Gudmundsson A (2011) Rock fractures in geological processes. Cambridge University Press

Gudmundsson A (2012) Magma chambers: formation, local stresses, excess pressures, and compartments. J Volcanol Geoth Res 237:19–41

Gudmundsson A (2020) Volcanotectonics: understanding the structure, deformation and dynamics of volcanoes. Cambridge University Press

Gudmundsson A, Brenner SL (2004) How mechanical layering affects local stresses, unrests, and eruptions of volcanoes. Geophys Res Lett 31(16)

Gudmundsson A, Brenner SL (2005) On the conditions of sheet injections and eruptions in stratovolcanoes. Bull Volcanol 67:768–782

Gudmundsson MT, Sigmundsson F, Björnsson H et al (2004) The 1996 eruption at Gjálp, Vatnajökull ice cap, Iceland: efficiency of heat transfer, ice deformation and subglacial water pressure. Bull Volcanol 66:46–65

Gudmundsson MT, Jónsdóttir K, Hooper A, Holohan EP et al (2016) Gradual caldera collapse at Bárdarbunga volcano, Iceland, regulated by lateral magma outflow. Science 353(6296):aaf8988

Gudmundsson A, Drymoni K, Browning J, Acocella V et al (2022) Volcanotectonics: the tectonics and physics of volcanoes and their eruption mechanics. Bullet Volcanol 84:1–8

Guest JE, Murray JB (1979) An analysis of hazard from Mount Etna volcano. J Geol Soc 136:347–354

Gurioli L, Sulpizio R, Cioni R, Sbrana A, Santacroce R, Luperini W, Andronico D (2010) Pyroclastic flow hazard assessment at Somma-Vesuvius based on the geological record. Bull Volcanol 72:1021–1038

Haeberli W, Beniston M (1998) Climate change and its impacts on glaciers and permafrost in the Alps. Ambio 27:258–265

Hall K (1982) Rapid deglaciation as an initiator of volcanic activity: an hypothesis. Earth Surf Proc Land 7:45–51

Hallet B, Hunter LE, Bogen J (1996) Rates of erosion and sediment evacuation by glaciers: a review of the evidence Global Planet. Change 12:213–235

Hardarson B, Fitton J (1991) Increased mantle melting beneath Snaefellsjökull volcano during Late Pleistocene deglaciation. Nature 353:62–64. https://doi.org/10.1038/353062a0

Harris C, Williams G, Brabham P, Eaton G, McCarroll D (1997) Glaciotectonized Quaternary sediments at Dinas Dinlle, Gwynedd, north Wales and their bearing on the style of deglaciation in the Eastern Irish Sea. Quatern Sci Rev 16:109–127

Hays JD, Imbrie J, Shackleton (1976) Variations in the Earth's orbit Pacemaker of the ice ages. Science 194:1121–1132

Healy D, Rizzo R, Duffy M, Farrell NJ, Hole MJ, Muirhead D (2018) Field evidence for the lateral emplacement of igneous dykes: implications for 3D mechanical models and the plumbing beneath fissure eruptions. Volcanica 1:85105

Heap MJ, Villeneuve M, Albino F et al (2020) Towards more realistic values of elastic moduli for volcano modelling. J Volcanol Geoth Res 390:106684

Heimdal TH, Svensen H, Ramezani J, Iyer K, Pereira E et al (2018) Large-scale sill emplacement in Brazil as a trigger for the end-Triassic crisis. Sci Rep 8:1–12

Hodgkins R, Carr S, Pálsson F, Guðmundsson S, Björnsson H (2013) Modelling variable glacier lapse rates using ERA-Interim reanalysis climatology: an evaluation at Vestari-Hagafellsjökull, Langjökull, Iceland. Int J Climatol 33:410–421

Hooper A, Ófeigsson B, Sigmundsson F, Lund B, Einarsson P, Geirsson H, Sturkell E (2011) Increased capture of magma in the crust promoted by ice-cap retreat in Iceland. Nat Geosci 4:783–786

Hunt AG, Malin PE (1998) Possible triggering of Heinrich events by ice-load-induced earthquakes. Nature 393:155–158

Hunt CB (1953) Geology and geography of the Henry Mountains region, Utah: a survey and restudy of one of the classic areas in geology (Vol. 228). US Government Printing Office

Huybers P, Langmuir C (2009) Feedback between deglaciation, volcanism, and atmospheric CO2. Earth Planet Sci Lett 286:479–491

Huybers P, Wunch C (2005) Obliquity pacing of the late Pleistocene glacial terminations. Nature 434:491–494

Forbes Inskip ND, Browning J, Meredith PG, Gudmundsson A (2020) Conditions for fracture arrest in layered rock sequences. Results Geophys Sci 1:100001

Jacoby W, Gudmundsson MT (2007) Hotspot Iceland: an introduction. J Geodyn 43:1–5

Jakobsson SP (1972) Chemistry and distribution pattern of recent basaltic rocks in Iceland. Lithos 5:365–386

James TS, Bent AL (1994) A comparison of eastern North American seismic strain-rates to glacial rebound strain-rates. Geophys Res Lett 21:2127–2130

Jamieson (1865) On the history of the last geological changes in Scotland. Geol Soc London Quart J 21:161–203

Jellinek AM, DePaolo DJ (2003) A model for the origin of large silicic magma chambers: precursors of caldera-forming eruptions. Bull Volcanol 65:363–381

Jellinek AM, Manga M, Saar MO (2004) Did melting glaciers cause volcanic eruptions in eastern California? Probing the mechanics of dike formation. J Geophys Res: Solid Earth 109(B9)

Johannesson H, Saemundsson K (1998) Geological map of Iceland. Tectonics, 2nd ed., Icelandic Institute of Natural History. scale: 500,000

Johnson AM, Pollard DD (1973) Mechanics of growth of some laccolithic intrusions in the Henry mountains, Utah, I: field observations, Gilbert's model, physical properties and flow of the magma. Tectonophysics 18:261–309

Jolly RJH, Sanderson DJ (1997) A Mohr circle construction for the opening of a pre-existing fracture. J Struct Geol 19:887–892

Jull M, McKenzie D (1996) The effect of deglaciation on mantle melting beneath Iceland. J Geophys Res 101:21815–21828

Kavanagh JL, Menand T, Sparks RSJ (2006) An experimental investigation of sill formation and propagation in layered elastic media. Earth Planet Sci Lett 245:799–813

Kavanagh JL, Roger BD, Boutelier D, Cruden AR (2017) Controls on sill and dyke-sill hybrid geometry and propagation in the crust: the role of fracture toughness. Tectonophysics 698:109–120

Kavanagh JL, Burns AJ, Hazim SH, Wood EP, Martin SA, Hignett S, Dennis DJ (2018) Challenging dyke ascent models using novel laboratory experiments: implications for reinterpreting evidence of magma ascent and volcanism. J Volcanol Geoth Res 354:87–101

Kavanagh JL (2018) Mechanisms of magma transport in the upper crust—dyking. In Volcanic and igneous plumbing systems. Elsevier

Koulakov I, Jakovlev A, Luehr BG (2009) Anisotropic structure beneath central Java from local earthquake tomography. Geochem Geophys Geosyst 10:2

Larsen CF, Motyka RJ, Freymuller JT, Echelmeyer KA, Ivins E (2005) Rapid viscoelastic uplift in southern Alaska caused by post Little ice Age glacial retreat, Earth Planet. Sci Lett 237:548–560

Larsen DJ, Geirsdóttir Á, Miller GH (2015) Precise chronology of Little Ice Age expansion and repetitive surges of Langjökull, central Iceland. Geology 43:167–170

Latychev K, Mitrovica JX, Tamisiea ME, Tromp J, Moucha R (2005) Influence of lithospheric thickness variations on 3-D crustal velocities due to glacial isostatic adjustment. Geophys Res Lett 32(1)

Lee JE, Shen A, Fox-Kemper B, Ming Y (2017) Hemispheric sea ice distribution sets the glacial tempo. Geophys Res Lett 44:1008–1014

Letourneur L, Peltier A, Staudacher T, Gudmundsson A (2008) The effects of rock heterogeneities on dyke paths and asymmetric ground deformation: the example of Piton de la Fournaise (Réunion Island). J Volcanol Geoth Res 173:289–302

Li S, Grapenthin R, Sigmundsson F, Drouin V, Hreinsdóttir S, Ófeigsson BG (2022) Post-rifting relaxation during 2015–2020 following the Bárðarbunga-Holuhraun dike intrusion and eruption in Iceland. Geophys Res Lett 49(13):e2022GL098977

Lund Snee JE, Zoback MD (2020) Multiscale variations of the crustal stress field throughout North America. Nat Commun 11:1–9

Lundgren P, Girona T, Bato MG, Realmuto VJ, Samsonov S, Cardona C, ... Aivazis M (2020) The dynamics of large silicic systems from satellite remote sensing observations: The intriguing case of Domuyo volcano, Argentina. Sci Rep 10(1):11642

Maccaferri F, Bonafede M, Rivalta E (2010) A numerical model of dyke propagation in layered elastic media Geophys. J Int 180:1107–1123

Maclennan J, Jull M, McKenzie D, Slater L, Grönvold K (2002) The link between volcanism and deglaciation in Iceland. Geochem Geophys Geosyst 3:1–25

Magee C, Stevenson C, O'driscoll B, Schofield N, McDermott K, (2012) An alternative emplacement model for the classic Ardnamurchan cone sheet swarm, NW Scotland, involving lateral magma supply via regional dykes. J Struct Geol 43:73–91

Magnússon E, Björnsson H, Dall J, Pálsson F (2005) The 20th century retreat of ice caps in Iceland derived from airborne SAR: W-Vatnajökull and N-Mýrdalsjökull. Earth Planet Sci Lett 237:508–515

Mathieu L, Burchardt S, Troll VR, Krumbholz M, Delcamp A (2015) Geological constraints on the dynamic emplacement f cone-sheets - the Ardnamurchan cone-sheet swarm, NW Scotland. J Struct Geol 80:133–141

Mattsson T, Burchardt S, Almqvist BS, Ronchin E (2018) Syn-emplacement fracturing in the Sandfell laccolith, eastern Iceland—implications for rhyolite intrusion growth and volcanic hazards. Front Earth Sci 6:5

McGuire WJ, Howard RJ, Firth CR et al (1997) Correlation between rate of seal level change and frequency of explosive volcanism in the Mediterranean. Nature 389:473–476

Menand T (2011) Physical controls and depth of emplacement of igneous bodies: a review. Tectonophysics 500:11–19

Milankovitch M (1930) In Handbuch der Klimatologie, edited by W. Koppen and R. Geiger, pp. 1–176, Gebruder Borntraeger, Berlin

Morner NA (1978) Faulting, fracturing, and seismicity as functions of glacio-isostasy in Fennoscandia. Geology 6:41–45

Mullet B, Segall P (2022) The surface deformation signature of a transcrustal, crystal mush-dominant magma system. J Geophys Res: Solid Earth 127:e2022JB024178

Óskarsson N, Steinthórsson S, Sigvaldason GE (1982) A dynamic model of rift zone petrogenesis and the regional petrology of Iceland. J Petrol 23:28–74. https://doi.org/10.1093/petrology/23.1.28

Óskarsson N, Steinthórsson S, Sigvaldason GE (1985) Iceland geochemical anomaly: origin, volcanotectonics, chemical fractionation and isotope evolution of the crust. J Geophys Res 90:10011. https://doi.org/10.1029/jb090ib12p10011

Pagli C, Sigmundsson F (2008) Will present day glacier retreat increase volcanic activity? Stress induced by recent glacier retreat and its effect on magmatism at the Vatnajökull ice cap, Iceland. Geophys Res Lett 35:9

Pagli C, Sigmundsson F, Lund B et al (2007) Glacio-isostatic deformation around the Vatnajokull ice cap, Iceland, induced by recent climate warming: GPS observations and finite element modeling. J Geophys Res 112:B08405

Pálmason G (1980) A continuum model of crustal generation in Iceland—kinematic aspects. J Geophys 47:7–18

Pasquaré Mariotto F, Bonali FL (2021) Virtual geosites as innovative tools for geoheritage popularization: a case study from eastern Iceland. Geosciences 11:149

Pasquarè FA, Tibaldi A (2007) Structure of a sheet-laccolith system revealing the interplay between tectonic and magma stresses at Stardalur Volcano, Iceland. J Volcanol Geotherm Res 161:131–150

Passerini P, Marcucci M, Sguazzoni G, Pecchioni E (1997) Longitudinal strike-slip faults in oceanic rifting: a mesostructural study from western to southeastern Iceland. Tectonophysics 269:65–89

Pfeffer W (2007) A simple mechanism for irreversible tidewater glacier retreat. J Geophys Res: Earth Surf 112:F3

Pinel V, Jaupart C (2004) Magma storage and horizontal dyke injection beneath a volcanic edifice. Earth Planet Sci Lett 221:245–262

Plateaux R, Béthoux N, Bergerat F, Mercier de Lépinay B (2014) Volcano-tectonic interactions revealed by inversion of focal mechanisms: stress field insight around and beneath the Vatnajökull ice cap in Iceland. Front Earth Sci 2:9

Poinar K, Joughin I, Das SB, Behn MD, Lenaerts JT, Van Den Broeke MR (2015) Limits to future expansion of surface-melt-enhanced ice flow into the interior of western Greenland. Geophys Res Lett 42:1800–1807

Pollard DD, Johnson AM (1973) Mechanics of growth of some laccolithic intrusions in the Henry Mountains, Utah II: bending and failure of overburden and sill formation. Tectonophysics 18:311–354

Rabatel A, Sanchez O, Vincent C, Six D (2018) Estimation of glacier thickness from surface mass balance and ice flow velocities: a case study on Argentière Glacier, France. Front Earth Sci 6:112

Rivera A, Bown F, Carrión D, Zenteno P (2012) Glacier responses to recent volcanic activity in Southern Chile. Environ Res Lett 7:014036

Rodríguez-Cardozo F, Hjörleifsdóttir V, Jónsdóttir K, Iglesias A et al (2021) The 2014–2015 complex collapse of the Bárðarbunga caldera, Iceland, revealed by seismic moment tensors. J Volcanol Geoth Res 416:107275

Roe GH, Baker MB, Herla F (2017) Centennial glacier retreat as categorical evidence of regional climate change. Nat Geosci 10:95–99

Roman-Berdiel T, Gapais D, Brun JP (1995) Analogue models of laccolith formation. J Struct Geol 17:1337–1346

Rosakis AJ, Samudrala O, Coker D (2000) Intersonic shear crack growth along weak planes Mater Res. Innovations 3:236–243

Schilling JG (1973) Icelandic mantle plume: geochemical evidence along Reykjanes Ridge. Nature 242:565–571

Schilling JG, Kingsley RH, Devine JD, Sigmundsson F (2006) Mantle plume-mid-ocean ridge interaction in the North Atlantic. Iceland geodynamics: crustal deformation and divergent plate tectonics 5–25

Schmiedel T, Galland O, Breitkreuz C (2017) Dynamics of sill and laccolith emplacement in the brittle crust: role of host rock strength and deformation mode. J Geophys Res: Solid Earth 122:8860–8871

Shackleton NJ (1987) Oxygen isotopes, ice volume and sea level. Quat Sci Rev 6:183–190

Sigmundsson F, Pinel V, Lund B, Albino F, Pagli C, Geirsson H et al (2010) Climate effects on volcanism: influence on magmatic systems of loading and unloading from ice mass variations with examples from Iceland. Phil Trans R Soc Lond 368:2519–2534

Sigmundsson F, Hooper A, Hreinsdóttir S et al (2015) Segmented lateral dyke growth in a rifting event at Bárðarbunga volcanic system, Iceland. Nature 517:191–195

Sigvaldason GE, Steinthórsson S (1974) Chemistry of tholeiitic basalts from Iceland and their relation to the Kverkfjöll hot spot. Geodynamics of Iceland and the North Atlantic Area. D. Reidel, Dordrecht, Holland, pp 155–164

Sigvaldason GE, Annertz K, Nilsson M (1992) Effect of glacier loading/deloading on volcanism: postglacial volcanic production rate of the Dyngjufjöll area, central Iceland. Bull Volcanol 54:385–392

Sinton J, Gronvold K, Saemundsson K (2005) Postglacial eruptive history of the western volcanic zone, Iceland. Geochem Geophys Geosyst 6:Q12009

Spaans K, Hooper A (2016) InSAR processing for volcano monitoring and other near-real time applications. J Geophys Res: Solid Earth 121:2947–2960

Spacapan JB, Galland O, Leanza HA, Planke S (2016) Control of strike-slip fault on dyke emplacement and morphology. J Geol Soc 173:573–576

Stephens TL, Walker RJ, Healy D, Bubeck A, England RW, McCaffrey KJ (2017) Igneous sills record far-field and near-field stress interactions during volcano construction: isle of Mull, Scotland. Earth Planet Sci Lett 478:159–174

Stewart IS, Sauber J, Ros J (2000) Glacio-seismotectonics: ice sheets, crustal deformation and seismicity. Quatern Sci Rev 19:1367–1389

Structural Module User's Guide (2021) COMSOL Multiphysics® v. 6.0. COMSOL AB, Stockholm, Sweden

Sulpizio R, Massaro S (2017) Influence of stress field changes on eruption initiation and dynamics: a review. Front Earth Sci 5:18

Thordarson T, Larsen G (2007) Volcanism in Iceland in historical time: volcano types, eruption styles and eruptive history. J Geodyn 43:118–152. https://doi.org/10.1016/j.jog.2006.09.005

Thordarsson T, Hoskuldsson A (2002) Iceland. In: Terra (Ed.), Classic geology in Europe

Tibaldi A (2015) Structure of volcano plumbing systems: a review of multi-parametric effects. J Volcanol Geotherm Res 298:85–135

Tibaldi A, Pasquaré F (2008) A new mode of inner volcano growth: the "flower intrusive structure". Earth Planet Sci Lett 271:202–208

Tibaldi A, Vezzoli L, Pasquaré FA, Rust D (2008) Strike-slip fault tectonics and the emplacement of sheet-laccolith systems: the Thverfell case study (SW Iceland). J Struct Geol 30:274–290

Tibaldi A, Bonali FL, Pasquaré F, Rust D, Cavallo A, D'urso A, (2013) Structure of regional dykes and local cone sheets in the Midhyrna-Lysuskard area, Snaefellsnes Peninsula (NW Iceland). Bull Volcanol 75:1–16

Tibaldi A, Bonali FL, Corti N, Russo E, Drymoni K et al (2022) Surface deformation during the 1928 fissure eruption of Mt. Etna (Italy): insights from field data and FEM numerical modelling. Tectonophysics 837:229468

Turcotte DL, Schubert G (2002) Geodynamics. Cambridge University Press

Valentine GA, Krogh KE (2006) Emplacement of shallow dikes and sills beneath a small basaltic volcanic center–the role of

pre-existing structure (Paiute Ridge, southern Nevada, USA). Earth Planet Sci Lett 246:217–230

Villemin T, Bergerat F, Angelier J, Lacasse C (1994) Brittle deformation and fracture patterns on oceanic rift shoulders: the Esja peninsula, SW Iceland. J Struct Geol 16:1641–1654

Walker GP (1982) Volcanic hazards. Interdisc Sci Rev 7:148–157

Walker RJ (2016) Controls on transgressive sill growth. Geology 44(2):99–102

Westerman DS, Rocchi S, Dini A, Farina F, Roni E (2015) Rise and fall of a multi-sheet intrusive complex, Elba Island, Italy. In: Breitkreuz, C., Rocchi, S. (eds) Physical geology of shallow magmatic systems. Advances in volcanology. Springer, Cham. https://doi.org/10.1007/11157_2014_5

White RS, Edmonds M, Maclennan J, Greenfield T, Agustsdottir T (2019) Melt movement through the Icelandic crust. Phil Trans R Soc A 377:20180010

Wilson AM, Russell JK (2020) Glacial pumping of a magma-charged lithosphere: a model for glaciovolcanic causality in magmatic arcs. Earth Planet Sci Lett 548:116500

Woods J, Winder T, White RS, Brandsdóttir B (2019) Evolution of a lateral dike intrusion revealed by relatively-relocated dike-induced earthquakes: the 2014–15 Bárðarbunga-Holuhraun rifting event, Iceland. Earth Planet Sci Lett 506:53–63

Yamasaki T, Kobayashi T, Wright TJ, Fukahata Y (2018) Viscoelastic crustal deformation by magmatic intrusion: a case study in the Kutcharo caldera, eastern Hokkaido, Japan. J Volcanol Geoth Res 349:128–145

Zoback MD (2010) Reservoir geomechanics. Cambridge University Press